MSc Thesis

Predicting Overpressures in Zechstein Stringers Based on Their Seismic Expression

Student	P.M. Schilder	**Daily Supervisor (EBN)**	G. Hoetz
Student Number	2525797	**Supervisor (VU)**	Dr. P.J.F. Verbeek
Date	January, 2019	**Second Assessor (VU)**	Prof. Dr. W. van Westrenen

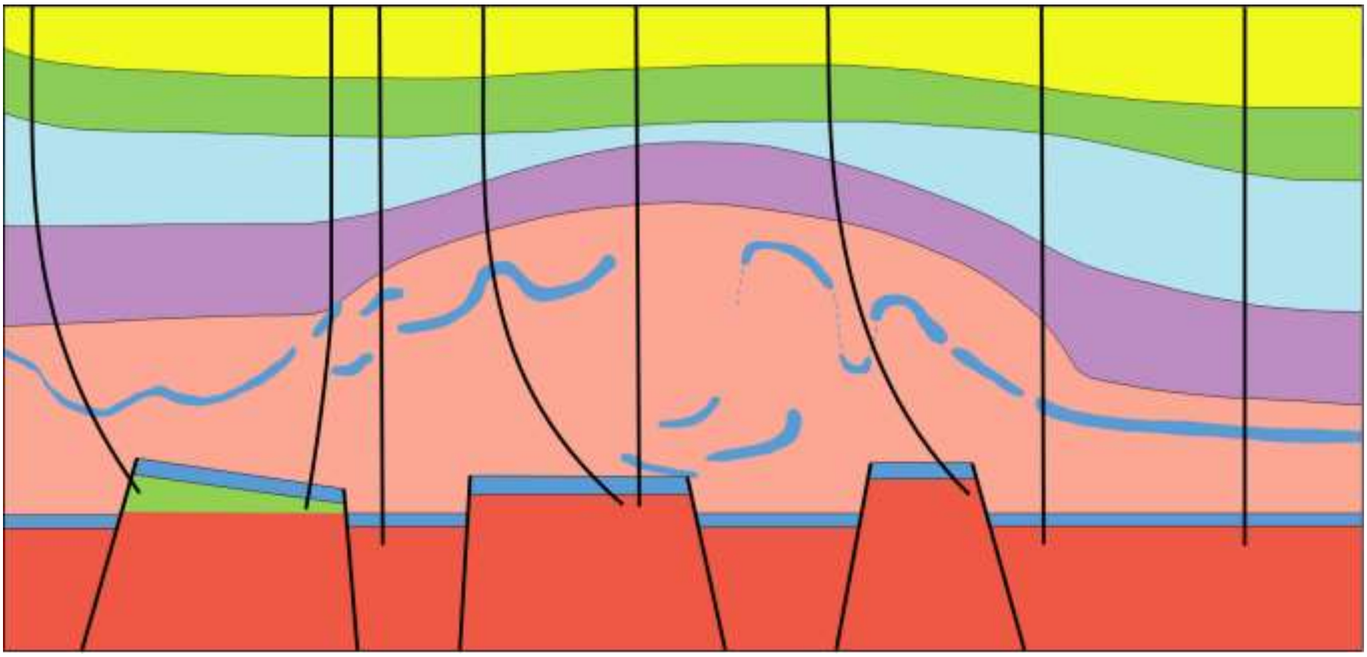

Master Thesis Earth Sciences, Specialisation Geology & Geochemistry, code AM_1186, 27 ECTS

Abstract

Late Permian Zechstein intra-salt bodies of the North Sea Basin represent a drilling risk, as they can be highly overpressured. Folded and boudinaged clay–carbonate–anhydrite bodies (termed 'Z3 stringers') isolated in halite are present throughout the Southern Permian Basin and can often not be avoided when targeting deeper reservoirs. This study assessed the predictability of overpressures in Z3 stringers based on their seismic expression. Energie Beheer Nederland, the Dutch state oil company, set up a database that currently contains information of about 960 Dutch wells that have been analysed for drilling events with a significant geological component in the cause. Included were 40 cases of Z3 stringer penetrations that showed pore pressures close to lithostatic, the majority of which were related to carbonates. Seismic expressions of Z3 stringers that are correlated with an increased chance of encountering overpressures include a small size (<1 km^2), areas of maximum curvature and areas within 300 m of a stringer's edge. These are areas of enhanced fracture porosity and permeability, particularly in the carbonates. Rock mechanics dictate that in a small volume of fractured material surrounded by an impermeable boundary, most of the stresses are applied to the pores, resulting in pore pressures up to lithostatic. The two proposed mechanisms of overpressure generation in the Zechstein are disequilibrium compaction through effective sealing of deformed Z3 stringers by halite and fluid expansion as a result of gas generation.

Contents

1.Introduction

1.1 Thesis Objectives

The sedimentary basins of NW Europe are classic areas of salt tectonics (**Van Gent et al., 2010**). Although these basins have been explored for several decades, debate continues regarding the depositional evolution and subsequent deformation of salt bodies. In the Dutch subsurface, five evaporite cycles of the Late Permian Zechstein Group (Z1–Z5) are recognized (**Geluk, 2007**). Included in the third cycle is a relatively brittle, folded and boudinaged, claystone–carbonate–anhydrite layer (the Z3 stringer) enclosed in ductile salt (**Geluk, 2005**). Z3 stringers not only are reservoirs for hydrocarbons but can also cause serious drilling problems. Events sometimes occur when drilling into stringers, which lead to non-productive time (NPT), safety risks and in more extreme cases can result into early abandonment of a well. The Z3 Carbonate Member (ZEZ3C) can be significantly overpressured, up to lithostatic (**Van Gent et al., 2010**). An example of such a stringer-related drilling event is described in the case study section below.

Case Study

With an average rate of penetration of 20.8 m/hr in anhydrite, drilling went well on 9th July 2017. However, at around 19:15 at a depth of 2828 m along hole, drilling parameters started to change. four more metres were drilled during which the torque erratically increased, circulating pressure increased from 165 to 215 bar, gas readings increased from 0 to 1.1% and claystone cuttings were coming up. The well was closed in and had gained 5 m^3 of formation fluids. Shut in drill pipe pressure and shut in casing pressure observed were 64 and 67 bar respectively. The mud weight was increased in steps from 1.51 to 1.91 s.g. in an attempt to regain well control, but after four days it was decided to plug the hole with cement and make a sidetrack. Total non-productive time and costs related to this event amounted to respectively 21 days and €6.1 million. As can be seen in the seismic image on the right it appears the well drilled a relatively small, i.e. <200 m, isolated, high-reflectivity feature, which is related to a Z3 stringer.

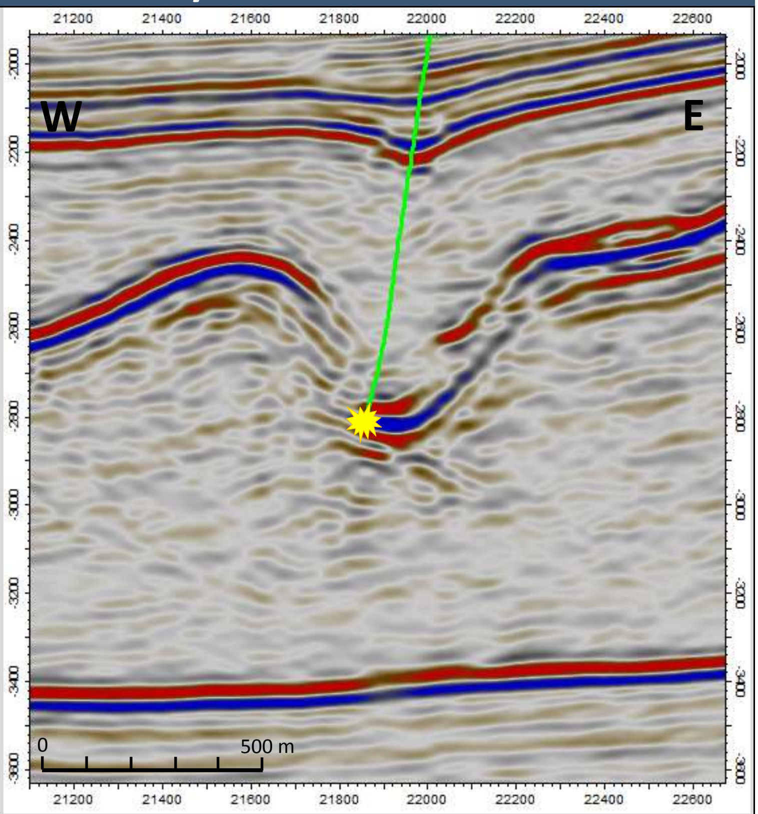

The main goal of this research is to *investigate whether overpressures in the Zechstein are predictable based on seismic expressions*. This might contribute to reduce both time and costs while drilling and guarantee safety on the rig. Particular attention will be given to Z3 stringers. This study concerns a Master Thesis that was performed as part of an MSc in Earth Sciences with a specialisation in Geology & Geochemistry at the VU University Amsterdam. The actual research was conducted at Energie Beheer Nederland B.V. (EBN) in Utrecht, the Netherlands. EBN is a company that invests in the exploration, extraction and storage of gas and oil on behalf of the Dutch State.

1.2 Geological Background

1.2.1 Tectonic Setting

The large-scale tectonic setting of the Netherlands and adjacent areas is driven by the N–S collision of Gondwana and Laurussia during the Late Carboniferous to form Pangea, and the subsequent rifting during the Triassic in the Arctic–North Atlantic and western Tethys domains. This formed, in conjunction with the anisotropic and thickened crust of the Variscan fold belt, a complex system of basins and rifts in NW Europe (**Geluk, 2005**). Alpine inversion of these basins took place during the Late Cretaceous and Early Paleogene as a result of the collision of Iberia and Europe. This was followed by Oligocene to recent development of the Rhine Graben rift system (**De Jager, 2007**).

Permian rocks in the Netherlands rest unconformably upon relatively mildly deformed Namurian to Stephanian sedimentary rocks. This unconformity represents a hiatus that comprises the entire Early Permian. In Middle and Late Permian times, the Netherlands became included in a large E–W trending complex of sedimentary basins, usually referred to as the Southern Permian Basin, stretching from the UK into Poland (**Fig. 1.2.1**). Situated at a palaeolatitude around 10° N during a hot and dry climate, it was bounded by the London-Brabant Massif and the Rhenish Massif to the south, and the Mid North Sea High and Ringkøbing-Fyn High to the north (**Geluk, 2007**). The stratigraphic nomenclature as used by TNO is followed.

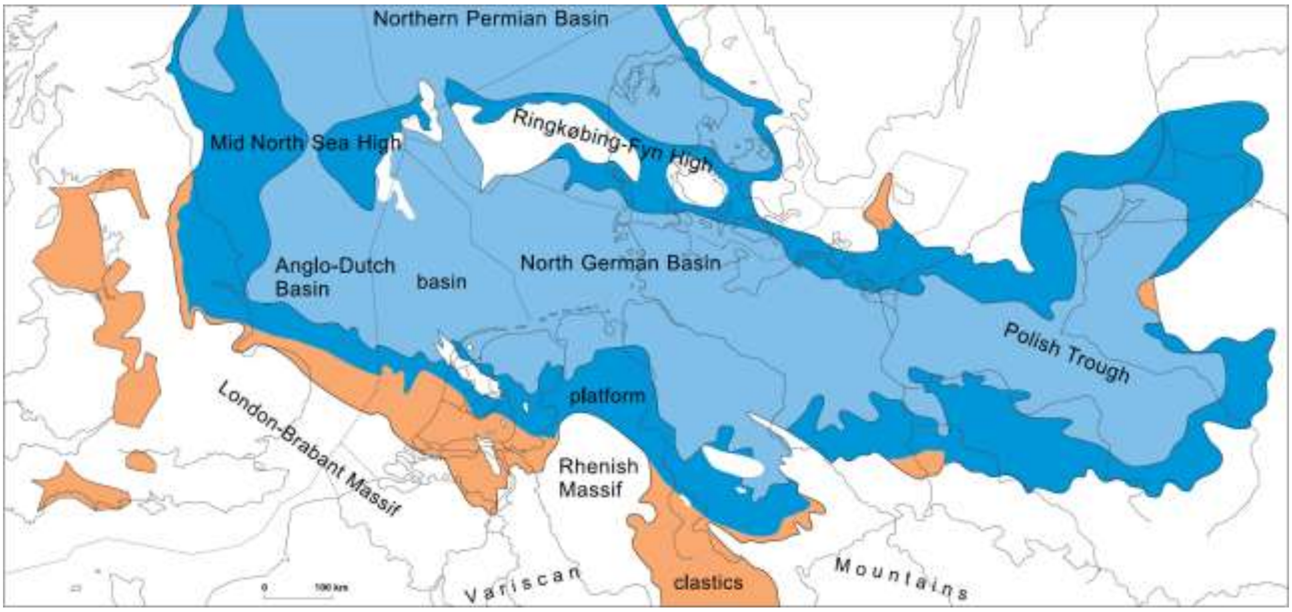

Fig. 1.2.1 Present-day distribution and facies map of the Zechstein Group (Z2 Carbonate, Late Permian) in the Southern Permian Basin (*after* ***Lokhorts, 1998; Taylor, 1998; Geluk, 2005***) *in* ***Geluk (2007)***.

1.2.2 Stratigraphy of the Zechstein Group

The Late Permian Zechstein Group (ZE Group) is subdivided into seven evaporite cycles (Z1–Z7), of which the lower five have been identified in the Dutch subsurface (**Fig. 1.2.2**, **Strozyk et al., 2012**). Z1–Z3 are considered marine deposits, whereas Z4–Z5 are regarded as playa-type deposits (**Geluk, 1997, 2000**). The typical evaporite cycle consists of claystone, followed by a carbonate phase, subsequent anhydrite precipitation, halite crystallisation, K–Mg rich salts, halite crystallisation and lastly anhydrite. Several of these classical cycles are identified within the ZE Group, but they often consist of multiple sub-cycles where one or more components may be missing (**Ligtenberg, 2007**). The depositional thickness of the ZE Group increases from less than 50 m in the southern Netherlands to over 1200 m in the northern offshore (**Geluk, 2007**) and is typically buried 1.5–3 km deep at present (**Strozyk et al., 2012**).

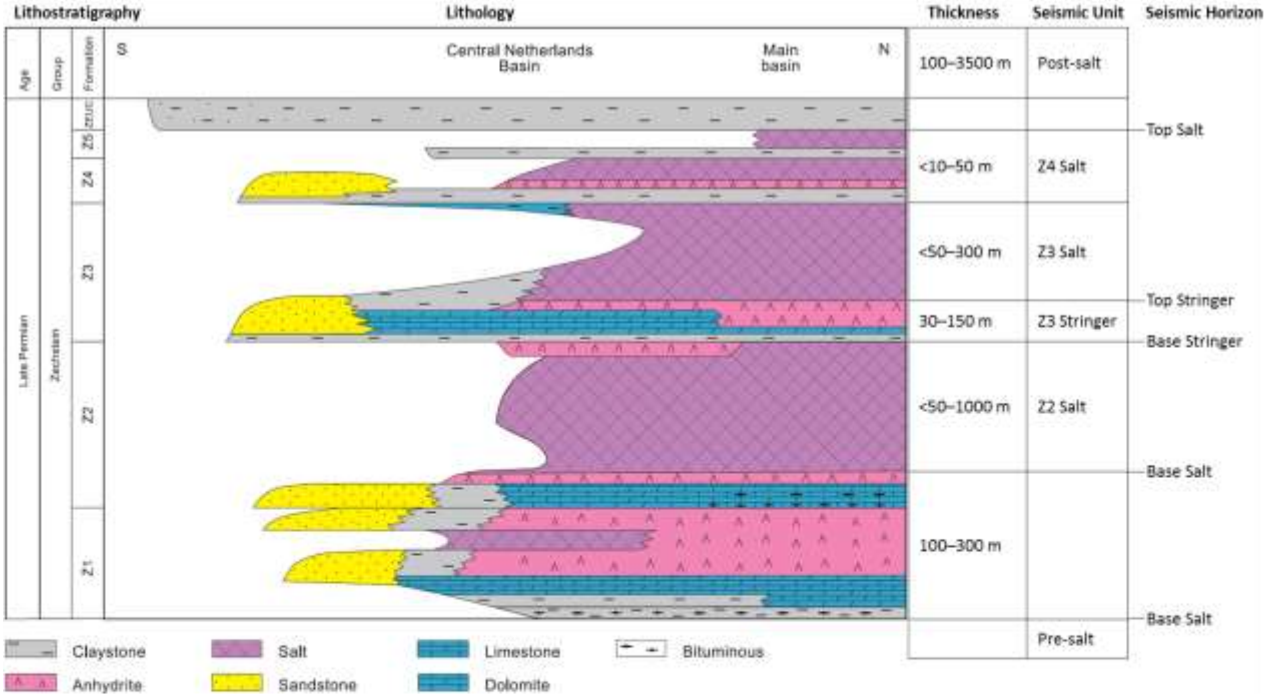

Fig. 1.2.2 Stratigraphic diagram of the Zechstein Group *after* ***Van Adrichem Boogaert & Kouwe (1994)*** *in* ***Geluk (2007)*** *and modified after* ***Zijp et al. (2018)***.

Deposition of the *Z1 (Werra) Formation* started with the Coppershale (ZEZ1K), a 0.5-m-thick claystone. It was deposited in most of the Netherlands, with the exception of the southern onshore area. Furthermore, the formation comprises the Z1 Carbonate Member (ZEZ1C), Z1 Anhydrite Member (ZEZ1W) and the Z1 Salt Member (ZEZ1H). It has a constant thickness of about 50 m in the basin, but can reach up to 500 m in the eastern part of the Netherlands where an anhydrite–carbonate platform developed (**Geluk, 2007**).

The *Z2 (Stassfurt) Formation* is typically comprised of the Z2 Carbonate Member (ZEZ2C), Z2 Basal Anhydrite Member (ZEZ2A) and the Z2 Salt Member (ZEZ2H). The formation is less than 50 m thick in the southern Netherlands and more than 700 m in the northern offshore. The topography of the ZEZ2C is thought to have controlled the thickness and distribution of the overlying units (**Geluk, 2007)**. Near the top of the ZEZ2H locally thick deposits of K–Mg salt layers are found. In addition, the Z2 Roof Anhydrite Member (ZEZ2T) is identified in some areas and forms the upper boundary of the Stassfurt Formation there. The ZEZ1H is absent in large parts of the Dutch subsurface. This means that the ZEZ2C and ZEZ2A lie directly on top of the ZEZ1W. Therefore, up to the ZEZ2A, all rocks are brittle and coupled to the Upper Rotliegend Group (RO) and underlying basement (**Van Gent et al., 2010**).

The Z3 Grey Salt Clay Member (ZEZ3G) forms the lower boundary of the *Z3 (Leine) Formation* and has a thickness of 1–10 m. Thickness estimates of the overlying Z3 Carbonate Member (ZEZ3C) range from 30 to 90 m on the slope to a few metres in the basin (**Geluk, 2007; Van Gent et al., 2010**). On top of the ZEZ3C lies the Z3 Main Anhydrite Member (ZEZ3A). The thickness of this member increases from 3 m on the slope to 45 m in the basin, with local excursions in excess of 100 m (**Van Gent et al., 2010; Zijp et al., 2018**). The Z3 Salt Member (ZEZ3H) is composed of a massive basal halite part and an upper section comprising two thick K–Mg salt layers. Higher-order salts encountered include bischofite, kieserite, carnallite and sylvite and are commonly known as 'squeezing salts'. The ZEZ3H is only present in the NE and NW offshore of the Netherlands and can reach 300–400 m in thickness (**Geluk, 2007**).

Within the ZEZ3C three facies realms are identified: platform, slope and basin. In N–S sections, at right angles to the basin axis, the carbonate unit seems to have a well-defined sigmoidal shape. This shape is thought to have formed as a result of the maximum thickness development being on the slope and transition to the platform. These facies prograded northward, shifting the area of maximum thickness northward with time (**Brooks et al., 1986; Geluk, 2007**). The basin facies comprises a dark-coloured limestone that has a thickness of a few metres to twelve metres and is suggested to have been deposited in a water depth of several tens of metres. This facies can have source-rock potential. Slumps consisting of displaced shelf deposits have been identified in the vicinity of slope and platform facies. The slope facies consists of laminated and bioturbated carbonate mudstones and silty dolomites (**Geluk, 2000**). Oolitic and bioclastic grainstones locally occur in the area adjacent to the slope and on the landward margin of the platform (**Zijp et al., 2018**). It can reach a thickness of up to 200 m and is sometimes characterised by redeposited platform sediments resulting from gravity flows. The platform facies is composed of microcrystalline dolomites and algal boundstones. In the western offshore area, the carbonate grades into fluvial sandstones. It can be up to 80 m in thickness locally and mainly consists of shallow-water deposits with occasional karst features (**Geluk, 2000**).

The thick and dominant claystone–carbonate–anhydrite portion of the Z3 cycle is relatively brittle compared to the surrounding halite. In large parts of the Dutch subsurface this competent layer has become fully encased in halite as a result of halokinesis and is commonly referred to as a 'raft' or a 'floater' (**Strozyk et al., 2012**). Although, these names imply buoyancy, carbonate and anhydrite typically have densities of 2.85 and 2.9 g/cc respectively, making them much denser than halite (2.2 g/cc). Therefore, Z3 stringers are expected to sink under the influence of gravity over geological time, provided that the rheology of the surrounding salt allows this to happen. For this reason, the term 'stringers' is preferred and will be used to describe such features in this report (**Van Gent et al., 2010**).

The *Z4 (Aller) Formation* is composed of a basal claystone, known as the Red Salt Clay Member (ZEZ4R), followed by the thin Z4 Pegmatite Anhydrite (ZEZ4A) and the Z4 Salt Member (ZEZ4H). The lower two members are distributed over a large area, whereas the ZEZ4H is only found in local depressions. K–Mg salts occur in the middle part of the ZEZ4H member and halite–claystone alternations occur in the upper part. The salt member reaches up to 150 m in thickness (**Geluk, 2007)**.

The occurrence of the *Z5 (Ohre) Formation* is limited to the NE onshore and NW offshore parts of the Dutch subsurface, outlining the depocentres towards the end of ZE sedimentation. The formation is comprised of a basal claystone of a few metres thick and up to 15 m of halite. The Z6 and Z7 are absent in the Netherlands, possibly as a result of non-deposition. The youngest ZE unit is the Zechstein Upper Claystone Formation (ZEUC) and disconformably overlies older strata. It is 10–50 m thick and is present in large portions of the Dutch subsurface (**Geluk, 2007)**.

1.2.3 Evaporite Basin Model

The 'classic' model of the evolution of evaporate basins is based on the deep-basin shallow-water model of **Hsü et al. (1973)**. This model assumes an initially deep basin and that its final thickness reflects initial basin depth (**Fig. 1.2.3*a***).

The formation of ZE halite bodies has also been attributed to deep-basin shallow-water deposition. Here, the estimate of maximum basin depth equals the thickness of the thickest halite body—the ZEZ2H—which can be up to 600 m thick. It is widely accepted that at the termination of each cycle, halite had filled the basin approximately to sea level, and that after continued tectonic subsidence the deposition of a subsequent evaporite cycle started.

Despite the wide acceptance of a deep-basin origin of halite bodies, several aspects of their formation have not been explained. A long list of arguments against a deep-basin shallow-water origin includes the unexpected occurrence of tidal sediments in evaporite basins. Although the model explains the occurrence of mainly shallow-water depositional structures, the model is qualified as unlikely in most tectonic environments, because it requires subsidence and deposition to be in equilibrium during the deposition of km-scale evaporite successions (**Van den Belt et al., 2007; *and references therein***).

The role of isostasy in evaporite basins is commonly not taken into account. **Van den Belt et al. (2007)** proposes isostatic compensation as a mechanism to create thick evaporite sequences in initially shallow-water basins (**Fig. 1.2.3*b***). Several authors have acknowledged the loading effect on the crust of thick sedimentary deposits (**Norman & Chase, 1986; Diegel et al., 1995 and Van Wees et al., 2000**), but have not considered it as a syn-depositional phenomenon in the case of evaporites.

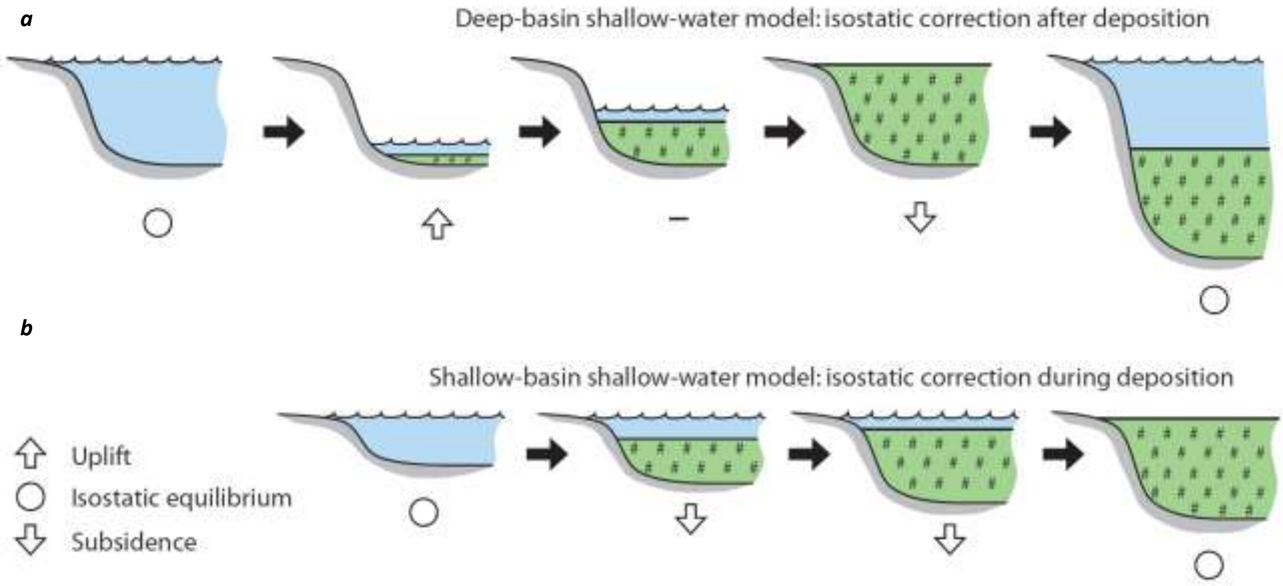

Fig. 1.2.3 ***a***) The deep-basin shallow-water model for saline giants is based on isostatic compensation after salt precipitation. ***b***) The shallow-basin shallow-water model for saline giants is based on isostatic compensation during salt precipitation. *After* ***Van den Belt et al. (2007)***.

The deep-basin theory that was developed for saline giants requires that the unusually steep basin margins as they are observed now in the subsurface were already in place before the onset of evaporite precipitation. If this were indeed the case, then the marginal successions within such basins would be characterised by abundant clastic deposits. However, evaporite cycles are characterised by an absence of clastic interbeds. It is therefore assumed that the tectonic component of total subsidence in most evaporite basins is low (**Van den Belt et al., 2007; *and references therein***).

The model of **Van den Belt et al. (2007)** assumes that most saline giants were deposited in initially shallow-basin shallow-waters. In this model the implications of syn-depositional isostatic compensation were assessed by making simple calculations based on the Airy isostasy model. Input values included the dimension of the Southern Permian Basin which was 300 x 1500 km (**Ziegler, 1990**). Late Permian ZE deposition lasted somewhere between 5 and 10 ma (**Menning, 1995; Krijgsman et al., 1999**) and isostatic compensation occurs on a scale of 10,000 years (**Watts, 2001**). In addition, precipitation rates of halite and gypsum/anhydrite are assumed to be in the order of 10–150 and 1–10 mm/yr respectively (**Van den Belt et al., 2007; *and references therein***). Thus, the precipitation rate for gypsum/anhydrite is in the same order as subsidence rates of extensional basins.

The model of **Van den Belt et al. (2007)** assumes syn-depositional isostatic compensation takes place. This shallow-basin model is more applicable and less restrictive where tectonic and geographical conditions are concerned. For example, it accounts for the occurrence of shallow-water sediments (early stage) as well as deeper-water sediments (late stage), without repetitive km-scale marine desiccation and re-filling. The main implication of isostatic compensation in evaporite-basin evolution is that evaporite precipitation drives subsidence instead of the opposite, and that thick halite deposits as they are observed in the rock record require an initial basin depth much less than their eventual thickness. Current depositional models depend on external control, whereas the mechanism proposed by **Van den Belt et al. (2007)** is self-regulatory, which explains why giant marine evaporites are so common in the rock record.

Van den Belt et al. (2007) propose a shallow-basin shallow-water model starts with a shallow-basin with initial topography. This basin starts out with clay on the margins and a carbonate platform that's thinning into the basin centre (**Fig. 1.2.4**). Major anhydrite bodies have been shown to be basin-margin wedges and the bulk of these bodies precipitated in shallow coastal sabkha environments. Evaporation has the greatest net effect in shallow-water and thus coastal platforms act as evaporite traps. Anhydrite precipitation on coastal platforms is probably biotically induced, whereas anhydrite varves in the basin centre are more likely to be chemically precipitated (**Kees van Oijk, personal communication, 2018**). These effects combined help explain why anhydrite deposits are thicker along the margins than in the basin centre.

Primary formation of anhydrite is inhibited by chemical boundary conditions, but primary gypsum may be directly converted into anhydrite under high temperature and/or high brine salinity, conditions commonly observed in coastal sabkha environments. Therefore, it is assumed that dehydration of gypsum takes place shortly after precipitation. Since the density of anhydrite is much higher than that of porous (siliciclastic) sediments surrounding the basin, it is expected that the anhydrite wedge will isostatically subside.

With subsequent evaporation, halite will start to precipitate. Since the precipitation rate for halite is in the order of 1–15 times higher than that of gypsum/anhydrite and isostatic subsidence rates, it can onlap onto the anhydrite and fill the basin to sea level. Isostatic compensation lags behind halite deposition and during that time—while the basin is slowly subsiding—the basin will be refilled with water and commonly clays. Subsequently, carbonates are deposited until the saturation rate of calcium sulphate has been reached again and sulphate will start to precipitate again.

A set of dimensional and compositional data for eighty-six Palaeozoic evaporite basins indicates that a minimum surface area of $\sim 3 \cdot 10^6\ km^2$ is required for halite saturation to occur. Progradation rates of anhydrite ramps in larger basins are higher because of a quadratic increase of surface area with basin circumference, hence more sulphate precipitates per unit shoreline. Corridors are therefore more rapidly closed. Due to faster closure, varve columns are thin in larger basins resulting in the typical steep slopes of evaporite platforms. Evaporite bodies in small basins are characterised by higher sulphate percentages, because prolonged sulphate precipitation leaves less space for subsequent halite and potash layers. As larger basins reach halite saturation quicker, ocean-corridor closure is less likely to be interrupted by subsidence events or sea-level rise.

The RO Aeolian sands, playa shales and evaporites that conformably underlie the ZE, and the overlying Triassic sediments were all deposited in a terrestrial environment. This suggests that tectonic subsidence was minor and that the ZE evaporites created their own accommodation space by means of loading (**Van den Belt et al., 2007; *and references therein***).

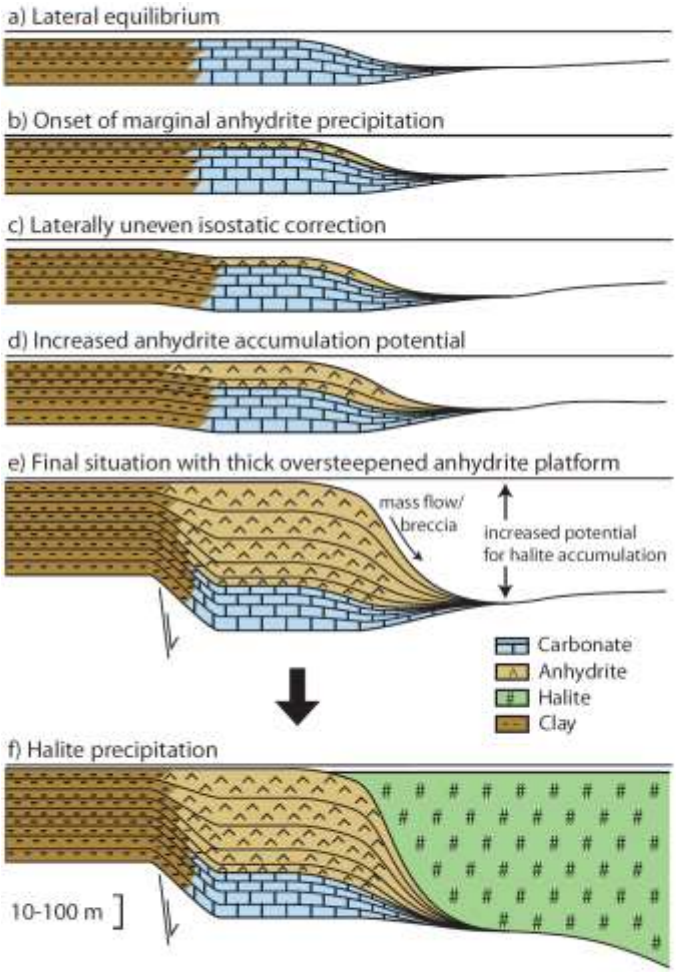

Fig. 1.2.4 Anhydrite precipitation model: the high density of anhydrite causes accelerated isostatic subsidence, thus allowing the accommodation of a thick anhydrite platform at the site of an initially shallow basin. On the other hand, anhydrite loading may result in the formation of a deep adjacent basin, which allows the consequent accumulation of a thick halite body. *After **Van den Belt et al. (2007)***.

1.2.4 Halokinesis

It is assumed that halokinesis was initiated by subsalt faulting that ultimately triggered differential loading by the overburden and resulted in salt withdrawal in basins and differently shaped salt structures (**Geluk, 2000**). Sediments of Mid Cenozoic age and younger are mostly undisturbed and almost horizontally layered, showing that large parts of the Dutch ZE have been tectonically inactive since the Paleogene, although some local salt movement still occurs today (**Geluk, 2007**; **Wong et al., 2007**).

According to **Taylor (1998)**, salt movement is mainly accommodated by flow of Z2 salt, while the Z3 and Z4 salts are more or less 'passively' displaced. Halokinesis strongly influenced the geometry of the Z3 stringer (**Fig. 1.2.5**), which shows a large variety of locally restricted and strongly varying deformation features, such as folding and boudinage associated with compression or shearing and extension or shearing, respectively. These features have been associated with the formation of salt domes, walls and pillows as well as extensional Z2 and Z3 salt thinning and supra-salt sediment basin growth. Similar structures have been observed in salt mines. Outcropping salt diapirs may represent analogues for buried salt structures (**Strozyk et al., 2012** ***and references therein***).

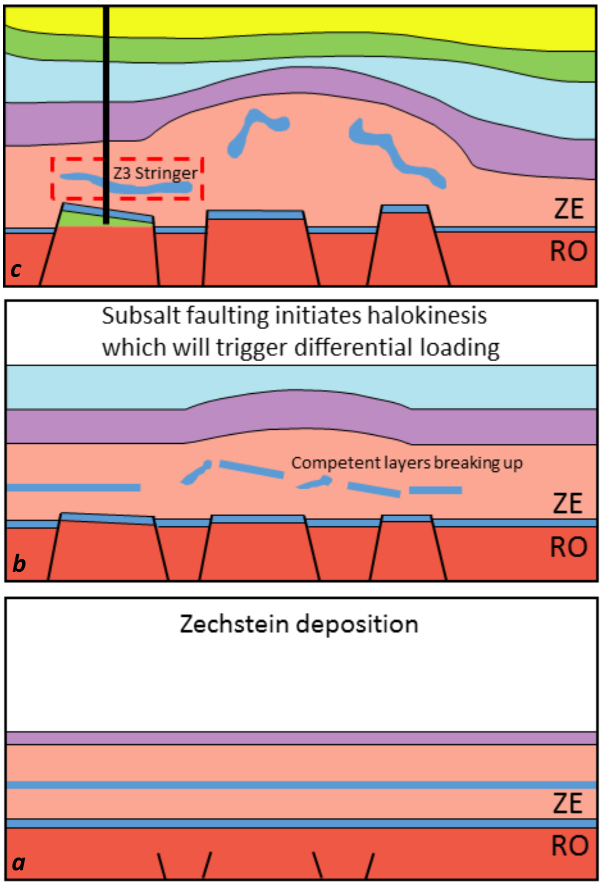

Fig. 1.2.5 ***a***) Schematic illustration of ZE deposition and ***b***) subsequent halokinesis, resulting in ***c***) isolation of the competent layers of the *Z3 (Leine) Formation*.

1.2.5 Principal Stresses

Before focussing on overpressures it is important to understand stresses. The following introduction to stresses is heavily based on **Zoback (2007)**. Stress is defined as a force acting over a given area. Forces in the Earth are quantified by means of a stress tensor, in which the individual components are tractions acting perpendicular or parallel to three planes that are in turn orthogonal to each other. For each point in space there is a particular stress axes orientation for which all shear stress components are zero and the *three principal stresses* $\sigma_1 \geq \sigma_2 \geq \sigma_3$ fully describe the stress field. The Earth's surface is in contact with a fluid (either air or water), which cannot support shear tractions, and is therefore a principal stress plane. Thus, one principal stress is generally normal to the Earth's surface with the other two principal stresses acting in an approximately horizontal plane. It has been found in most parts of the world that these stress conditions exist down to depths of about 15–20 km.

The Dutch subsurface is characterised by a normal faulting regime in the Anderson classification scheme, which defines the horizontal principal stress magnitudes with respect to the vertical stress. In a normal faulting regime, the vertical stress (σ_v) is the maximum principal stress (σ_1) and the horizontal stresses σ_H and σ_h are respectively σ_2 and σ_3.

The magnitude of σ_v is equivalent to integration of rock densities from the surface to the depth of interest and represents the *lithostatic stress* or *lithostatic gradient*. Typical values for the lithostatic in sedimentary basins range from 2.0 bar/10 m to 2.3 bar/10 m (e.g. **Gaarenstroom et al., 1993; Zoback, 2007; Kukla et al., 2011; Zijp et al., 2018**) and generally increases with depth. The range of possible values of σ_H and σ_h in a normal faulting regime is established by the fact that σ_h must always exceed the pore pressure (to avoid hydraulic fracturing). When there are severely overpressured formations at depth there are consequently small differences among the three principle stresses.

Because principal stresses are perpendicular and parallel to any plane without shear stress, the orientation of principal stresses is likely to be affected by the presence of salt bodies. Such bodies are so weak that there can be essentially no shear stress acting on the interface between the salt and the adjacent formations. This means that there will be a tendency for principal stresses to re-orient themselves to be parallel and perpendicular to these weak planes.

1.2.6 Pore Pressures

Pore pressure is defined as a scalar hydraulic potential acting within an interconnected pore space at depth. The value of pore pressure at depth is usually described in relation to *hydrostatic* or *normal pressure*; the pressure associated with a column of water from the surface to the depth of interest. The hydrostatic pore pressure at a certain depth is a function of water density, which in turn is dependent on temperature and composition. The hydrostatic gradient is about 1.0 bar/10 m and increases to 1.1 with depth as salinity increases (**Zoback, 2007**).

Overpressures are defined as pore pressures that exceed the hydrostatic at a given depth. Conceptually, the upper bound for pore pressure is the vertical stress. In addition, the pore pressure must always be lower than σ_3. Overpressures are generally considered to be generated by two distinct mechanisms *(1)* disequilibrium compaction or *(2)* fluid expansion (**Tingay et al., 2013**). In order for the fluid pressures to rise, the pressures have to be retained by rocks with sufficiently low permeability. Overpressures are transient and gradually leak away over geological time when the generation mechanisms cease to operate (**Kukla et al., 2011**). Most overpressures in sedimentary basins are generated by *(1)* undercompaction, in which overpressure is the result of loading through burial or high horizontal stresses of effectively sealed sediments. Fluid expansion overpressuring *(2)* comprises a suite of mechanisms in which the relative volume of pore fluid increases within a confined volume of sedimentary rock. The only mechanisms able to produce high-magnitude overpressures are thought to be load transfer *(1)*, vertical transfer *(1)* or the generation of gas *(2)*. Maturation of kerogen into gas can result in a large fluid volume increase of up to 50%, while cracking of only 1% of a volume of oil within a sealed rock could theoretically generate lithostatic overpressures (**Tingay et al., 2013**).

Pore pressures in Z3 stringers are primarily controlled by the geological burial history of ZE evaporites, movement of stringers within the ZE, and the specific mechanical and sealing properties of the salt surrounding stringers. The following main processes are thought to form overpressures in ZE stringers (**Zijp et al., 2018 *and references therein***):

- *(1)* Undercompaction resulting from rapid burial which prevents pore fluid from escaping to the surface;
- *(1)* Sealing of carbonates by overlying anhydrite and surrounding halite, and cementation leading to compartmentalization by seepage of anhydrite into the carbonate;
- *(1)* Stress-induced porosity reduction due to poroelastic effects or pressure solution.
- *(2)* Changes in pore fluid composition, e.g. the generation of hydrocarbons and sour gas in the carbonates;
- *(2)* Dehydration of gypsum.

Most of these processes only generate significant overpressures if the stringers are hydrologically disconnected from their surroundings by impermeable salt. Halokinesis caused fragments of the competent layers of the *Z3 (Leine) Formation* to become enclosed in ductile salt. This resulted in pore pressures that can exceed the hydrostatic (**Zijp et al., 2018**). Overpressured stringers within the Ara salts of Oman illustrate the ability of evaporites to maintain seal integrity over time frames of 250–500 ma (**Warren, 2016**).

Knowledge of the least principal stress provides important information for drilling stable wells (**Zoback, 2007**). Drilling mud is applied in the form of mud pressure (**Zhang & Yin, 2018**) and must be kept below σ_3 to prevent hydraulic fracturing and lost circulation, but above the pore pressure to support borehole walls, for preventing formation fluid influx and wellbore collapse during drilling (**Zoback, 2007; Zhang & Yin, 2018**).

When pore pressure found within the drilled rock is higher than the mud hydrostatic pressure acting on the borehole or rock face, formation fluids are forced into the wellbore, provided that porosity and permeability are sufficient. This may lead to a well control problem and if the situation can be contained the event is termed a *kick* or a *gain*. If not, a blowout may ensue. Anomalous pore pressures in the ZE are especially problematic when both over-and underpressures are encountered in an open-hole section, as no single mud weight is appropriate to handle both conditions in a single well (**Zijp et al., 2018**).

1.3 Geo-Drilling Events and NPT

A large number of wells has been drilled in the Dutch subsurface for varying purposes and by multiple operators. Wells covering both on- and offshore Dutch territory often had target depths of over 3 km. In addition, the Netherlands is densely populated, necessitating deviation of onshore well trajectories. Careful planning is required to drill (such) wells both cost and time efficiently as well as safe.

Numerous events occurred during the process of drilling a well. The origin of these drilling events can be found in a wide range of processes, which can be categorized according to three general factors: organisational, engineering and geology (**Fig. 1.3.1**). Most commonly, drilling incidents result from a combination of these factors. Organizational causes can be linked to human errors, such as operational judgement mistakes and engineering issues can be caused by mechanical equipment failure. This study focusses on geo-drilling hazards, which are related to drilling incidents that have a significant geological component in the cause, called 'Geo-Drilling Events' (GDE's). Geoscientists are required to identify and analyse the nature of GDE's in order to understand the underlying geological hazard.

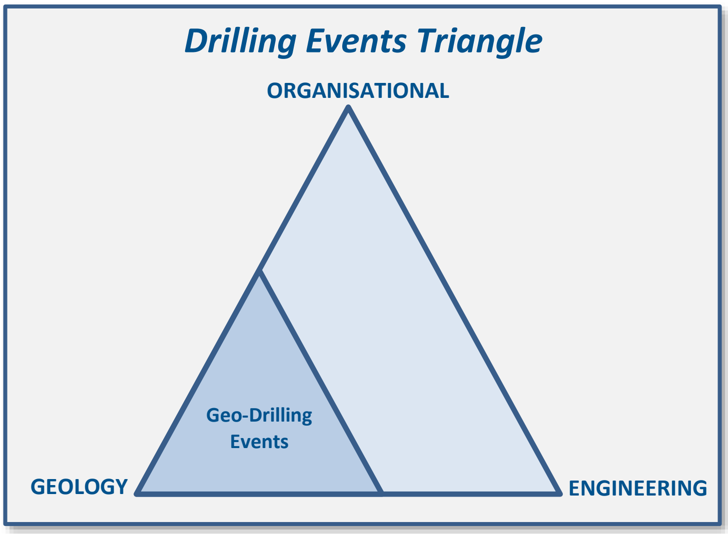

Fig. 1.3.1 Ternary diagram showing the three factors that can lead to drilling events and which can be plotted anywhere in this triangle based on their nature. Geo-Drilling Events have a significant geological component in their cause. *After* ***Hoetz et al. (2013)***.

GDE's lead to an increase in non-productive time (NPT) and in more extreme cases to the abandonment of a well. From a total of 5437 (**EBN** as per December, 2018) boreholes drilled for E&P purposes in the Netherlands, 1538 (**TNO** as per December, 2018) are sidetracks. It is likely that the majority of these sidetracks had to be drilled as a result of GDE's (see **Example #1**).

Example #1

EBN has monitored the lead time of executed wells in the period 2007–2017 and has divided the process of drilling a well into five phases. The second phase is called the 'dry hole time' (DHT) (**Fig. 1.3.2**) and is defined as the time between spudding and the moment TD is reached and the bit finished drilling and is pulled out of hole back to the rotary table. 310 wells have been drilled within this 10-year-period. Twelve wells with very long DHT's have been analysed in detail and the cause of the delays has been determined. It turns out that the delay for 10 out of these 12 wells (83%) is caused by geology-related problems.

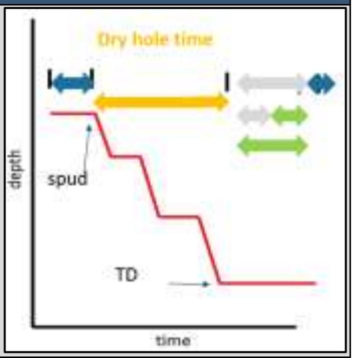

Fig. 1.3.2 after Slabbekoorn (2018)

In an attempt to improve well safety and reduce NPT related to GDE's, EBN B.V. captured GDE's that occurred in the Dutch subsurface in a database for easy access. Generally operators are reluctant to share subsurface information as they consider well data confidential. The involvement of EBN as a partner, rather than an operator in most wells, offers a position in which EBN has a good overview of the drilling performance throughout the Netherlands.

GDE's included in the database have so far been described according to descriptions found in well reports, drilling reports and composite logs. The inspection of seismic can help the understanding of certain GDE's, as illustrated by **Baud (2018)** who looked for seismic clues related to drilling fluid losses. The objective of this research is to analyse gains in the context of seismic. The main goal is to assess the predictability of Zechstein overpressures based on seismic expressions. Particular attention will be given to overpressures in isolated Z3 stringers. The hypothesis is that an above-average amount of overpressured stringers either have a small size or are penetrated in areas of maximum curvature. This relationship has never been tested properly using a statistical approach. Therefore, this research could open up the door to test this hypothesis and could evolve into a set of rules which enable the predictability of geo-drilling hazards in the planning phase of a well.

It is often assumed that once Z3 stringers become fully encased in halite, their pore pressures approach lithostatic stresses (e.g. **Van Gent et al., 2010; Kukla et al., 2011; Zijp et al., 2018**). If such high overpressures were not anticipated for while drilling, formation fluids can flow into the borehole. Formation fluid gains are considered a well control incident and have to be managed carefully. As such, they can lead to an increase in NPT and costs of the drilling phase (see **Example #2**). From an operator's perspective, it is very useful to predict geo-drilling hazards by taking structural information from seismic into account. In addition, an analysis using seismic data can provide more information on the geological cause of the GDE.

Example #2

Slabbekoorn (2018) investigated the number of 'High-Impact Events' that were encountered in specific stratigraphic (super)groups in 70 Dutch offshore wells with RO or DC targets that had a spud depth of 0 m and were drilled in the period 2007–2017 (**Fig 1.3.3*a***). The figure shows that 36 (40%) High-Impact Events took place in the ZE.
The average DHT days for the same set off wells has been determined for *(1)* wells that experienced 'No–Low-Impact Events' and *(2)* 'Medium–High-Impact Events' and is illustrated in **Fig 1.3.3*b***. This figure shows that there is a 44% increase in DHT days in wells that experienced Medium–High-Impact Events.
Fig. 1.3.3*c* and **1.3.3*d*** show respectively the average metres drilled per day and average costs per metre drilled for the same set of wells—which have an average effective along hole length of 4943 m. In case wells were sidetracked, only the length of the completed borehole is taken into account and not the cumulative metres drilled in all sidetracks. These figures show a decrease of 29% in metres per day drilled and an increase in cost of 61% per metre respectively when comparing wells that experienced No–Low-Impact Events with Medium–High-Impact Events.

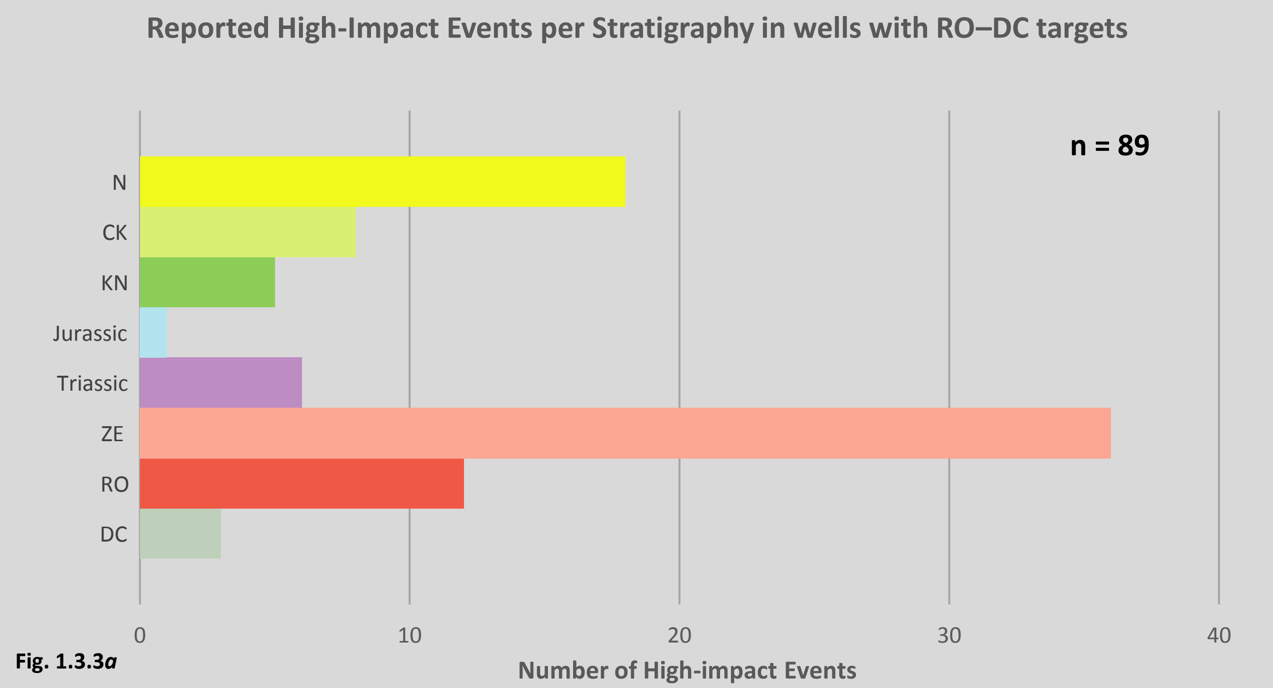

Fig. 1.3.3*a*

Dry Hole Time days for boreholes with RO–DC Targets

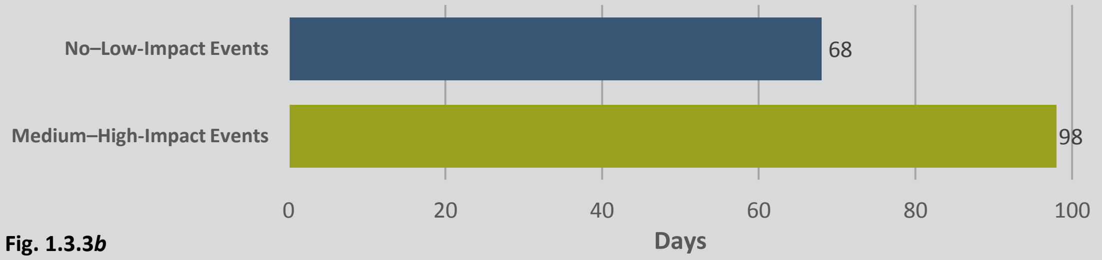

Fig. 1.3.3*b*

Average m/day drilled for boreholes with RO–DC targets

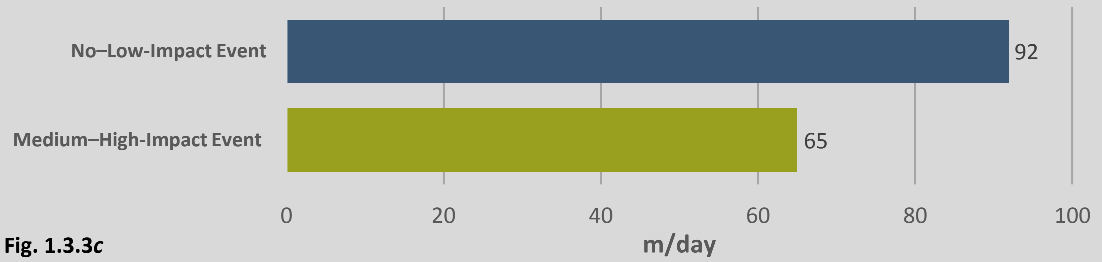

Fig. 1.3.3*c*

Average costs per m drilled for RO–DC targets

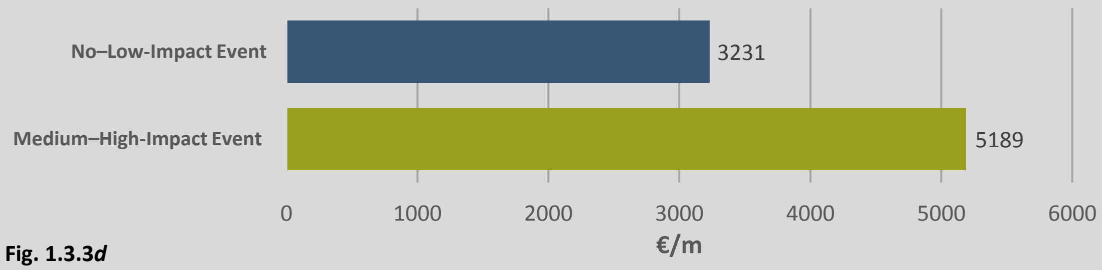

Fig. 1.3.3*d*

2. Methodologies

2.1 Geo-Drilling Events Database

The setup of the Geo-Drilling Events database is accurately described by **Kuiper (2017)** and subsequently updated by **Baud (2018)**. The description of events per well is divided into four main pillars:

- Generic well data: including basic well data;
- Geo-Drilling Event: an objective description of the type of event;
- Geo-Drilling Hazard: a description of the underlying geological cause of the GDE;
- References: the references used to describe the GDE and its hazard.

The GDE's and geo-drilling hazards are categorized according to the classification schemes shown in **Fig. 2.1*a*** and **2.2** respectively. Note that these schemes are based on event- and hazard-types that have been encountered in the Netherlands so far. New types of events and hazards might be identified in the future. The guidelines of the severity of the incidents are described per GDE-type, giving an indication on the impact of the event (**Fig. 2.1*b***). The impact of an event is determined by factors including incurred time and cost, and safety. To unlock the database for operators, the GDE information is imported into a specifically designed TIBCO Spotfire interface. This tool provides a user-friendly interface, which can be used to analyse the collected dataset. Changes to the internal interface are made by an assigned project engineer who can upload the interface to a cloud-environment for external usage. The Spotfire interface is comprised of four tabs, each providing a different visualization of the database. The interface can be accessed by account owners through: http://analytics.ebn.nl/spotfire/, and is explained in more detail in **Kuiper (2017)** and **Baud (2018)**.

By January 2019, the database included 960 analysed boreholes with 1171 GDE's recorded. As per December 2018, 6489 boreholes have been drilled in the Netherlands (**EBN internal database**). The number of GDE's included in the database is therefore expected to increase. However, not all wells were drilled for exploration purposes and wells drilled before 1960 often lack data of the drilling process. Hence, information about possible GDE's encountered during the drilling phase of these old wells was not always documented. The ultimate goal is to include at least one third of the total number of boreholes drilled in the Netherlands in the database to have a representative dataset that is suitable for statistically sound analysis.

In this regard, the first step of this research included expanding the GDE Database. GDE's were identified and subsequently analysed using well- and drilling reports available on NLOG and the local databases of EBN. Newly examined wells and adjusted GDE's already in the database are listed in **Appendix A**. To ensure good data integrity, new entries in the database are carefully reviewed by an experienced analyst before being released to partners/operators. All ZE gains that were already incorporated into the GDE database were meticulously double checked and an effort was made to identify more before importing them into Petrel, which will be discussed in the next section. The workflow of expanding the GDE database and subsequent analysis of a subset of the data is summarized in **Fig. 2.3**.

Gaining experience with the Spotfire interface was required, in order to improve it where deemed necessary and to be able to demonstrate its uses to parties both internally and externally. In addition, active participation was taken in the improvement of the workflow of entering new GDE's into the database, as it was transferred from an Excel environment to a Mendix environment.

Geo-Drilling Event Classification

GDE_CODE	GDE_Type	GDE Description
	Hole Geometry	
1	**Stuck Tubular/Tool**	Stuck pipe and/or excessive overpull and/or torque of the drill string or casing. Incidents may include: - Stuck pipe occurance during the drilling phase - Casing stuck and/or prematurely set due to no further progress while running in - Hole pack-off - Excessive reaming and/or hole cleaning required in combination with excessive overpull/torque - Differential sticking - Obstruction running liner or casing in the hole - Stuck logging tool (with the exception of a washout)
2	**Clay Balling**	Swelling and sticking clay causing: - a packed off drilling assembly - blocked flowline/flowriser - inability to continue drilling (no ROP)
3	**ROP**	Excessive wear of the drill bit resulting in reduced rate of penetration and/or excessive number of bit trips Unexpected reduction in ROP resulting in significant delay
11	**Steering**	Difficulties while steering the drilling assembly during drilling, either in rotary or sliding mode. For example due to formation change or formation dip angle
10	**Washout**	Unconsolidated formation, collapsing into the hole. Washed out formations as a result of mud type or excessive local circulation, possibly in combination with (anomalous) geology
9	**Deformed Tubular**	Deformed or collapsed casing/liner/tubing during well contruction or re-entry of an existing well, possibly in combination with (anomalous) geology.
	Pressures	
4	**Gain**	Flow of formation fluid into the borehole during well construction
5	**Losses**	Lost drilling fluids and/or cement into the formation during well construction
	Geology and Fluids	
7	**HC**	The unpredicted occurance of hydrocarbons while drilling
8	**H2S**	The unpredicted occurance of H2S while drilling
6	**Lithology**	Unexpected and/or unpredicted formation encountered while drilling Actual formation depth significantly different than proposed
12	**Other**	Other geological-related incidents that cannot be caterogized by any other code in this table **Note: Non-geological drilling incidents are not recorded in this database**

Fig 2.1*a* EBN's classification scheme of GDE's. A description of each GDE type is given as well.

Severity Guidelines

High	Medium	Low
examples	examples	examples
Lost drilling assembly in hole Prematurely set casing string in different than planned formation with effect on shoe strength Prematurely set casing string	Excessive jarring, reaming and/or circulation required Differential sticking requiring to spot a light fluid (e.g. base oil) pill to reduce overbalance Hole obstruction during casing running requiring an additional BHA check trip or opening up the hole	Excessive torque and/or overpull, but manageable
Lost tophole and/or sidetracked due to pack off and subsequent stuck pipe	Significant time delay due to clay balling Multiple trips required High-volumes swabbing occurence due to clay balling	Clay balling occurence but manageable
Excessive number of bit trips required due to extreme bit wear	Multiple bit trips required due to excessive bit wear	Reduced ROP and significant bit wear observed
Failed to reach objective	Steering difficulties, multiple BHA's required. Trajectory outside targetbox (at objective)	Steering difficulties, more time required to steer BHA
Washout resulting in accidential sidetrack Washouts resulting in insufficient cement around casing or liner	Washout resulting in significant quality loss of logging results	Washout requiring additional reaming or working of pipe/tools
Deformed casing/liner/tubing resulting in - significant operational delay (> 5 days NPT) - Complete loss of functionality of well	Deformed casing/liner/tubing resulting in - moderate operational delay (1-5 days NPT) - partial loss of functionality of well	Deformed casing/liner/tubing resulting in - minimum operational delay (< 1 day NPT) - no loss of functionality of well
Influx exceeding kick tolerance Kick-loss situation Well Control situation resulting in >5 days regaining well control Kick resulting in prematurely setting casing	Well control situation requiring well to be circulated to heavier fluid in controlled manner (over the choke) High pressures requiring a contingency liner to be set to allow drilling ahead	Able to control influx whilst drilling ahead Increased mud weight to overbalance formation pressure
Total losses, unable to keep the hole full Total losses leading to a kick/loss situation Losses during cement job resulting in lower TOC than planned Losses compromising section target Losses resulting in prematurely setting casing	Numerous LCM pills required to cure losses Gunk and/or cement pills required to cure losses	Losses curable whilst drilling (eg. By adding LCM material)
Mitigating the unpredicted occurance of HCs giving rise to - significant operational delay (> 5 days NPT) - Complete loss of functionality of well - Prematurely setting casing	Mitigating the unpredicted occurance of HCs giving rise to moderate operational delay (1-5 days NPT)	Mitigating the unpredicted occurance of HCs giving rise to minimum operational delay (< 1 day NPT)
Mitigating the unpredicted occurance of H2S giving rise to - significant operational delay (> 5 days NPT) - Complete loss of functionality of well - Prematurely setting casing	Mitigating the unpredicted occurance of H2S giving rise to moderate operational delay (1-5 days NPT)	Mitigating the unpredicted occurance of H2S giving rise to minimum operational delay (< 1 day NPT)
Missed final drilling target Failed to find objective	Found objective but after significant delay e.g. after sidetrack	E.g. Formation coming in significantly deeper or shallower than proposed (>100m) but no compromises on well design and/or target missed

Fig 2.1*b* Guidelines indicating the impacts of an event, which can be used to group the severity of an event into three categories.

Geo-Drilling Hazard Classification

HAZ CODE	HAZ Type	Description
	Rocks	
F	**Fault** (Faults/fractures in the borehole)	Destabilised rocks due to (natural) faulting/ fracturing. Resulting in anomalously high permeability (losses) and/or excessive cuttings/ cavings. Note that karstification might show up similarly as faults but is strictly spoken a different geological phenomena (see R)
C	**Swelling Clay** (Chemically unstable sediments)	Reactive formations (eg. swelling clays)
S	**Squeezing Salt** (Unstable evaporites)	Borehole formation deforming caused by high (litho) pressures mobilising evaporites
W	**Unstable Sediment** (Mechanically unstable sediments)	Unconsolidated formation (eg. washouts) Cavings due to high pressure Weak zones in formation
B	**Boulders**	Large detached rocks in borehole, typically originating from conglomerate
R	**Rock Properties** (Unexpected hard/soft or unexpected permeable)	Unexpected hard or soft formations Abrasive formation causing excessive bit wear Steering difficulties due to soft/hard alternation Dip angle
	Fluids	
D	**Depleted Reservoir**	Low reservoir pressure (e.g. due to nearby production)
E	**Shallow Gas**	Unexpected gas shows at shallow depths
G	**Anomalous Pressures**	Unexpected or unpredicted high or low geopressures: High pressures exceeding expected formation pressures (e.g. unexpected brine flows, brine pockets) Formation fluid pressures lower than expected (e.g. unexpected depletion due to nearby production)
H	**H2S**	Unexpected occurrence of hydrogensulfide gas in borehole
	Other	
M	**Mapping Uncertainty**	Unexpected formations Subsurface mapping is generally based on well and/or seismic data. Results are based on interpretation and can contain errors or has large uncertainty. Structural complexity, T2D conversion, flanks, unexpected fault/offset
Z	**Other / Unknown** (Other/Unknown Geo Hazard)	Other geological hazard (e.g. unconformities) or unknown geological hazard.

Fig 2.2 Classification and description of the Geo-Drilling Hazard types, representing the underlying geological cause of GDE's.

2.2 Further Research

Gains were visualized on seismic and well logs using Petrel 2016 (Schlumberger). After having scrupulously reviewed the ZE Gains already incorporated into the GDE Database, they were imported into Petrel as both point well data and well tops. The former allowed for different grouping- and visualization possibilities with respect to well tops. The latter allowed for a depth-to-time conversion by using the time–depth (T–D) relations of the wells which gained formation fluids.

In case a sonic log was run in a borehole, this log was calibrated with check-shots to get to a T–D relation. A sonic log is a type of acoustic log that displays travel time of P-waves versus depth. When such a log was not run, only check-shots were used to establish a T–D relation. If neither sonic logs, nor check-shots were available, a T–D relation was established by using one from nearby wells, typically in conjunction with TWT base surfaces made by TNO and by manually picking marker horizons. **Appendix B** shows how the T–D relation was established per well. When applicable, the lack of deviation data for a certain well is also mentioned in **Appendix B**.

Gain events—and corresponding wells, well tops and logs—have been visualized on seismic cross-sections in two directions; one perpendicular and the other parallel to large-scale structural elements at the ZE interval. Screenshots of these visualizations have been taken and are bundled together in a portfolio (**Appendix C**). The sections intersect gains, and in the case of highly deviated wells it therefore seems the seismic-to-well tie might be off, but this is simply due to projection. Unless stated otherwise, seismic is visualized in time domain with 5 times vertical exaggeration. Since gains are recorded in measured depth along a borehole with respect to the rotary table, proper deviation data and T–D relations are required to be able to accurately plot them in time domain. Most T–D relations of analysed wells lack sonic log data and therefore rely primarily on check-shots which relate a limited number of depths to specific time values. As a result, uncertainties exist in the T–D relation in between check-shots of a well. Therefore, an uncertainty range of ±50 ms is used when plotting gains in time domain. This value of ±50 ms is based on a study by **Hoetz (2016)**. TWT-surfaces of Top CK, ZE and RO are seismic interpretations by TNO. Well tops are from TNO and adjusted by EBN where needed. For some gains, cross-sections displaying relative acoustic impedance (IA) are included. Red loops on seismic and IA have a negative amplitude and represent a hard kick (unless stated otherwise).
In this study a set of seismic features is defined that could potentially predict the existence of overpressures in the ZE. This data has been compiled into **Appendix B**. The table consists of 6 parts:

- General Data: depth and severity of the gain and stratigraphy as per NLOG;
- Well Data: including reliability of the T–D relation, interpreted stratigraphy, stringer depth and thickness, fluid type, volume and/or concentration, kill mud gradient and pore pressure;
- Seismic Data: name and quality of seismic (cube) used;
- Stringer Data: descriptions of its geometry;
- Zechstein Data: descriptions of the circumjacent ZE geometry;
- Additional Data: comments, seismic domain and whether IA sections are included in **Appendix C**.

Firstly, it was determined from which ZE member a gain likely originated by combining data from the GDE database with seismic. After having identified the flows that emanated from Z3 stringers, the table was populated with descriptions of the seismic character of these stringers. Seismic expressions that have been categorized include:

1) Visibility
2) Continuity
3) Edge Proximity
4) Relative Depth
5) Dip
6) Shape

In addition, the kill mud gradient, pore pressure and distance (in TVD) between top ZE and gain have been added to the database for all ZE gains, as well as the depth of a stringer relative to top and base ZE. A legend and appendix are included in the database (**Appendix B**) in which a succinct description is given of the seismic features and how they were categorized. Further background on the rationale for capturing specific characteristics is given below.

(1) The high acoustic impedance contrast between the stringer and surrounding halite makes the Z3 stringer image rather well on seismic. Imaging limitations are related to the frequency content and noise level of the seismic data, to the thickness of the layer and to the local dip of the layer. When the thickness of the stringer is below the tuning range of about 30–35 m, exact thickness determination from seismic is not possible. Sections of the stringer with a thickness below ~10 m are not resolved. In addition, it may not be deposited in certain locations or it may be discontinuous after being disrupted by tectonic deformation (**Van Gent et al., 2010**).

(2) It is assumed (**Hoetz, 2018, personal communication**) that small stringers are more prone to hard overpressures than large slabs, since extensive stringers are more likely to have a potential leaking path. In addition, boudinaging of the competent layers of the *Z3 (Leine) Formation* could have created a fracture network that increased porosity and permeability. In contrast, continuous Z3 stringers ostensibly experienced less deformation and in turn, no increased porosity and permeability was created. *(3)* The same train of thought is related to the distance between drilling location and edge of the stringer.

(4) Z3 stringers show deformation features in large areas of the Dutch subsurface. The degree of folding and depth of Z3 stringers relative to top and base ZE is thought to be a proxy for the amount of deformation the stringer got exposed to and 'sinking' it experienced. The original stratigraphic position of the Z3 stringer is thought to be about 200–300 m below top ZE (**Van Gent et al., 2010**), which is within the upper third of the ZE in relative terms (**Zijp et al., 2018**). *(5)* The dip of a stringer's enveloping surface could be correlated to the amount of deformation and sinking of a stringer as well. *(6)* Flexural stretching near the hinge of folds may occur, opening up pre-existing fractures or creating additional ones as a result (**Peacock & Mann, 2005**). Consequently, porosity and permeability could be enhanced. It is important to bear in mind that the above seismic expressions could theoretically result in pressure kicks. The purpose of this study is to test these theoretical relationships by applying a statistical approach.

Kill mud gradients or equivalent mud weight (in s.g.) were taken from drilling reports if available and subsequently converted to pore pressures. It is generally assumed (**Hoetz, 2018, personal communication**) that at least a certain thickness of impermeable halite is needed to generate hard overpressures (up to lithostatic). Therefore, the distance between the depth (in TVD) of top ZE and the gain was calculated. If specified, fluid type is also included in the database (**Appendix B**). The assumption is that gases (hydrocarbons and sour gases) primarily originate from the carbonate members of the ZE Group or the underburden.

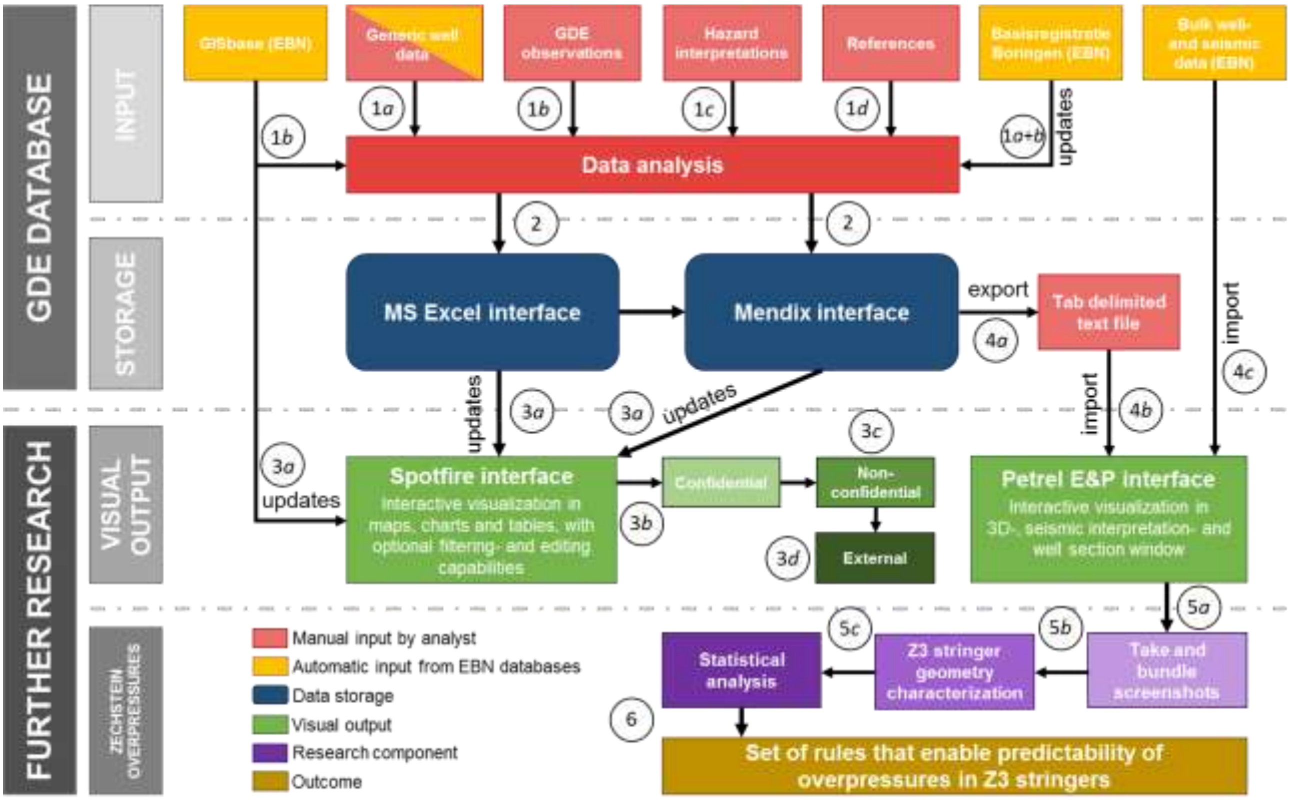

Fig. 2.3 Workflow of the GDE database and further research into overpressures in Z3 stringers. Up till January 2019, storage of GDE data was done in an MS Excel interface. Since then, storage is transferred to a Mendix interface. The advantage of a Mendix interface is that it is easier to link databases and it facilitates robust quality control. Circled numbers represent steps in the workflow, which include **1**) Data analysis: ***a***) manual input of generic well data by the analyst, as given on NLOG. With the transfer from Excel to Mendix, this step is now obsolete, as generic well data is now automatically imported from the EBN database “Basisregistratie Boringen” (BRB). ***b***) Data analysis of well reports from NLOG and EBN’s internal databases. Manual input of GDE observations by analyst. Deviation values and surface location of wells are automatically imported from BRB to calculate mTVDss and coordinates of GDE at depth. Stratigraphy is automatically imported from the GISbase (EBN) based on depth of GDE. ***c***) Interpretation by analyst of underlying geological cause of GDE using well logs, deviation and stratigraphic data. ***d***) Include references and mark initials of analyst and QC’er. **2**) Storage of GDE data, formerly in a MS Excel interface and since 2019 in a Mendix interface. **3*a***) Initially, this step included manual import by the analyst of the excel file into a specifically designed TIBO Spotfire interface. Since 2019, this step is carried out by a designated IT specialist. In the same project, GIS base layers are automatically imported from the GISbase and include map layers, blocks, sub-blocks, regions, boreholes (NL), oil- and gas fields, prospects and licences. **3*b***) The Spotfire project is for internal use only and offers an interactive visualization in maps, charts and tables, with filtering- and editing capabilities. This particular version includes confidential data. **3*c***) Confidential data is filtered out. **3*d***) Non-confidential data is uploaded to a cloud-environment for external use. **4*a***) Manual export of text file by analyst. Adjustment of format according to the needs and requirements set by the user/project. **4*b***) Manual import of exported text file into the Petrel E&P interface by the analyst as both well tops and point well data. Importing data as well tops enables GDE’s to be converted from depth to time domain, whereas importing data as point well data allows for convenient grouping and visualization possibilities. **4*c***) Manual import of relevant well and seismic data. This step included proper depth-to-time conversion of well trajectories. **5*a***) Gains were visualized on seismic, of which screenshots were taken. These screenshots are bundled in a MS PowerPoint interface (**Appendix C**). **5*b***) Based on well and seismic data it was determined which gains originated from Z3 stringers. A set of seismic features was defined that could potentially predict overpressures in Z3 stringers. This data is compiled in a MS Excel interface (**Appendix B**), together with relevant information from the GDE database. **5*c***) Statistical analysis was carried out on the seismic characteristics of Z3 stringers. **6**) this has resulted in a set of rules that enable predictability of overpressures in Z3 stringers based on their seismic expression.

3. Results

3.1 Zechstein Gains

A total of 960 boreholes has been investigated and incorporated into the GDE database, in which 68 cases with ZE gains have been identified. **Fig. 3.1.1*a*** shows the distribution of all ZE gains coloured according to their severity and **3.1.1*b*** shows the distribution of all ZE gains coloured according to the stratigraphic member from which they originated. There seems to be no clear correlation between severity and stratigraphic member. Note that some boreholes encountered more than one gain level. Twenty-seven gain events occurred onshore, compared to forty-one offshore. Fifty-nine percent of the gain events emanated from Z3 stringers (**Fig. 3.1.2*a***). The distribution of Z3 stringer kicks is displayed in **Fig. 3.1.1*c***. Out of all stringers drilled in the Netherlands, at least 3% flowed. This percentage is based on the total number of boreholes drilled in the Netherlands—including confidential wells with EBN participation—which amounts to 6489, as per December 2018. Stratigraphy is defined for 6011 of these boreholes, as per November 2017. Of these, 2031 are conclusive, meaning they drilled sufficiently deep into the ZE stratigraphy to drill the Z3 stringer if present. From these 2031 boreholes, a total number of 1321 encountered ZEZ3A/B/C and 40 of them flowed (**Fig. 3.1.2*b***).

Another significant portion (16%) of ZE overpressures was observed in the ZEZ2C, and together the carbonate members (Z1–Z3) accounted for 66% of the kicks. **Fig. 3.1.1*d*** displays the distribution of gains from the ZEZ1C, ZEZ2C and ZEZ3C. Note that ZEZ2C gains are localized mainly near the NE onshore part of the Netherlands. It is worth noting that in all cases of ZEZ2A/C gains, no ZEZ1H was encountered. This means that in these locations the *Z2 (Stassfurt) Formation* is expected to be in direct contact with the underburden.

The main fluids that fill up the pore spaces of a sedimentary rock include liquids such as brine and oil, and gases such as hydrocarbon gas, carbon dioxide, hydrogen sulphide, helium and nitrogen (**Zijp et al., 2018**). The number of gain events with a defined fluid type amounts to 65 (**Fig. 3.1.2*c***). A subdivision is made in the following fluid types; 'Brine', 'Gas', 'Brine & Gas', 'Brine & H_2S' and 'Gas & H_2S'. In this category, 'Gas' refers to natural gas, which is a mixture consisting primarily of methane, but commonly includes varying amounts of other higher alkanes (C_{1-x}). Gases may be entrained in brines, which fit into the categories 'Brine & Gas' and 'Brine and H_2S'. Pressure kicks are commonly divided into brine kicks and gas kicks. In this report, gas kicks are defined as any kick that included Gas or H_2S. A total of 26 gas kicks were identified, of which 14 and 12 occurred respectively onshore and offshore. Twenty of these gas kicks originated from the ZE carbonate members (**Fig. 3.1.2*d***). It is noteworthy that all onshore ZEZ2C kicks (8 out of 8) contained gases, compared to 1 out of 3 offshore. In relative terms, ZEZ2C kicks had the highest occurrences (82%) of gases.

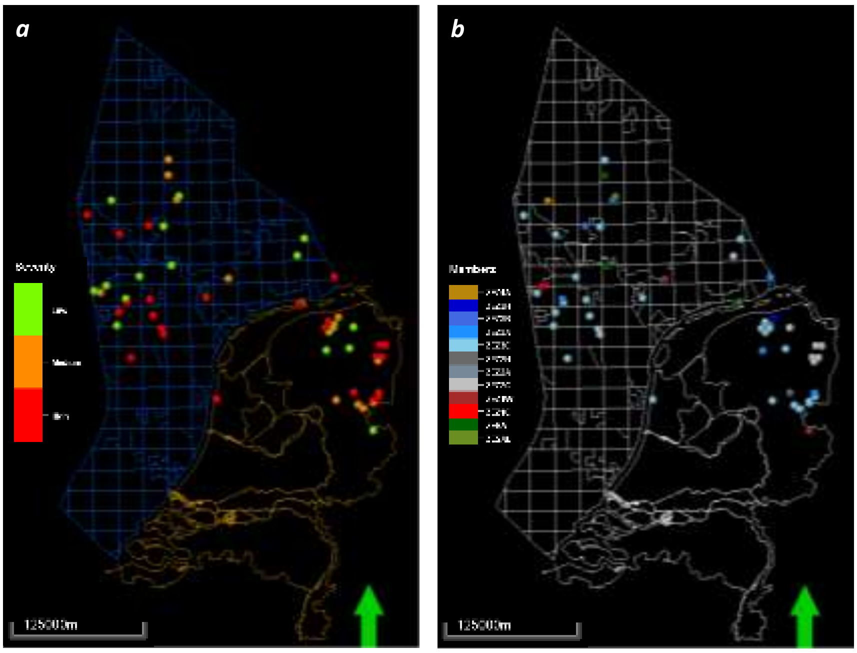

Fig. 3.1.1 *a*) Map view of the Netherlands and ZE gains distribution coloured according to their severity.

b) Map view of the Netherlands and ZE gains distribution coloured according to the stratigraphic members in which they occurred.

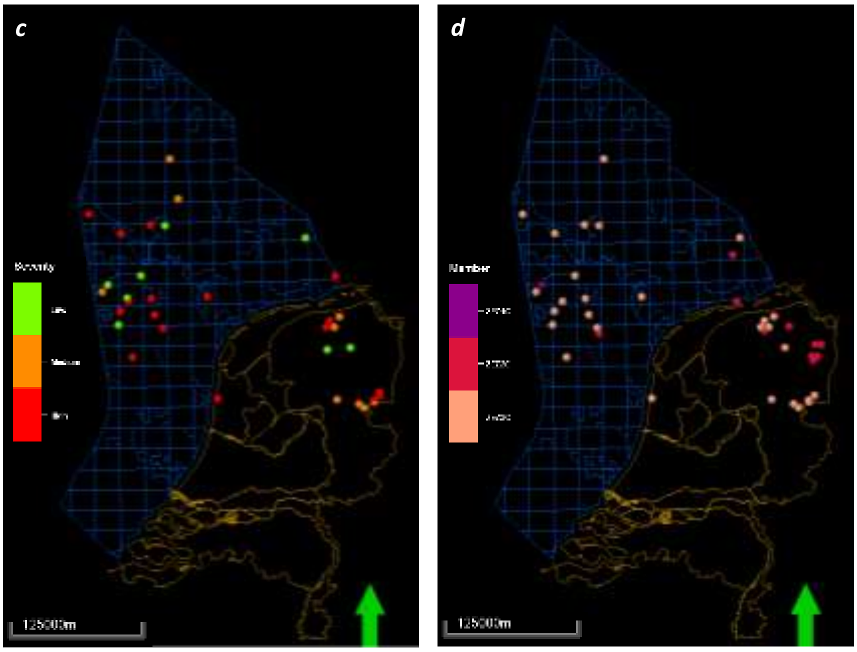

Fig. 3.1.1 ***c***) Map view of the Netherlands and Z3 stringer gains distribution coloured according to their severity.

d) Map view of the Netherlands and carbonate ZE gains distribution coloured according to their stratigraphic member.

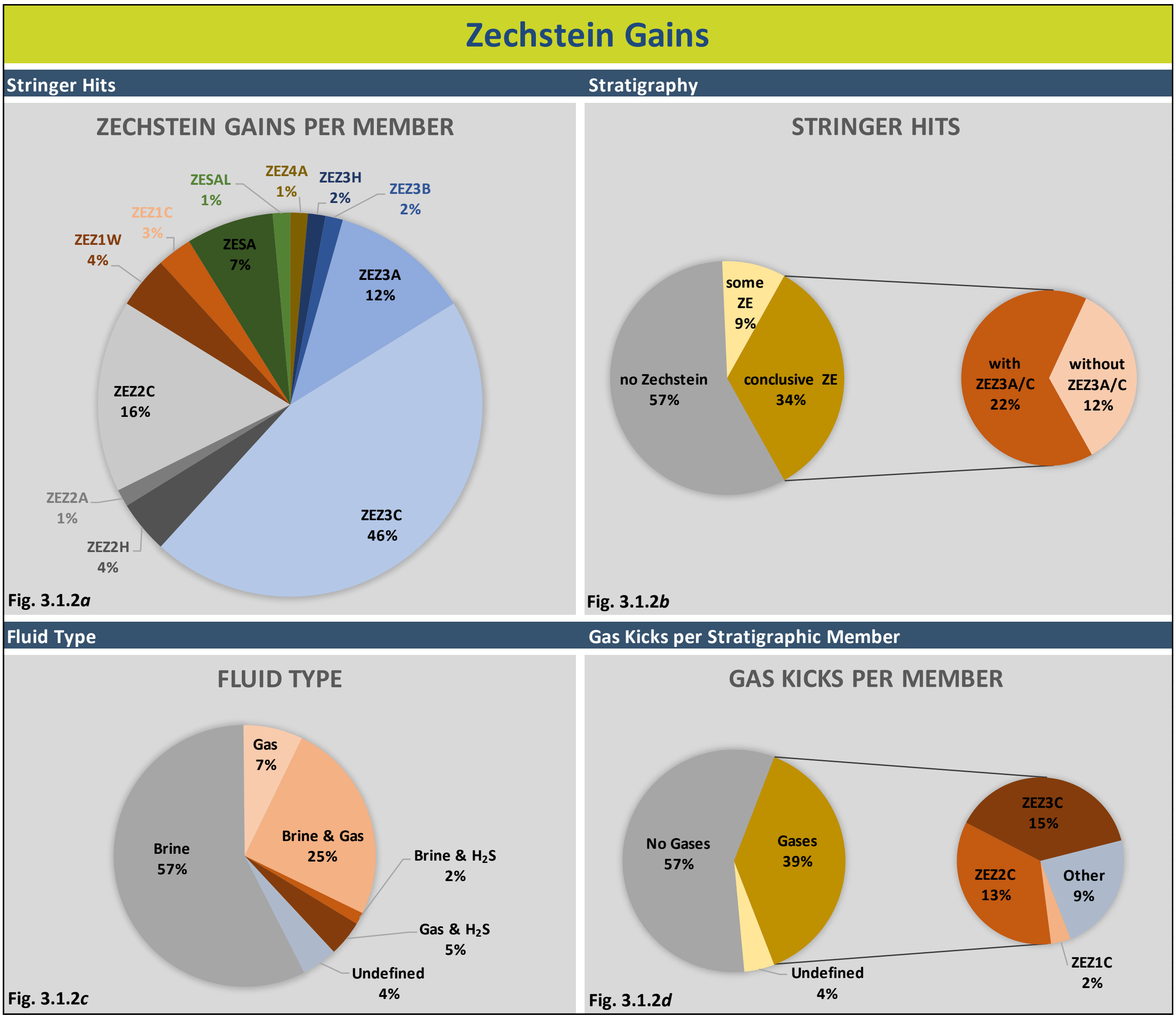

Fig. 3.1.2 ***a***) Pie chart showing the relative amount of ZE gains per stratigraphic member. (***b***) Pie of pie chart showing the relative number of boreholes that were conclusive and encountered ZEZ3A/C. (***c***) Pie chart illustrating the fluid type of kicks. (***d***) Pie of pie chart illustrating the relative amount of gas kicks that originated from ZE carbonate members.

3.2 Seismic Expression

Well data was correlated with seismic data in order to characterise seismic expressions for a total of forty flowing and nine non-flowing Z3 stringers. These characterizations are compiled in **Appendix B** and **C** and the results are summarized in **Table 1**. Examples of these seismic expressions are presented in **Fig. 3.2*a–d***. Below follows a comprehensive description of the main results.

(1) Visibility

The visibility of stringers on seismic could be determined for 36 out of 40 flowing and 8 out of 9 non-flowing stringers. In four cases both the seismic quality and T–D relationships were considered too poor for further characterization. Flowing and non-flowing stringers were visible on seismic in thirty-one and seven cases respectively. For the remaining cases, the well logs and cuttings proved Z3 stringers were drilled and that they were not visible on seismic.

(2) Continuity

The size of stringers has been determined by estimating the surface of a stringer. This was established by multiplying the longest axes in x–y direction and assuming the stringer has a rectangle shape. Subsequently, the continuity of Z3 stringers has been classified as 'Low', 'Medium' and 'High' which corresponds to an area of <1.0 km, 1–10 km and >10 km respectively. Continuity could be determined for thirty flowing and six non-flowing stringers. 73% of the stringers that kicked had a low continuity. In contrast, only 17% of the non-flowing Z3 stringers had a low continuity. Ten flowing and three non-flowing Z3 stringers were deemed inconclusive, as it was not possible to give an adequate estimation of their continuity. This was mainly due to a poor T–D relation and seismic quality and low visibility of the stringers. In the case of the non-flowing Z3 stringer penetrated by well TUM-01, the continuity could not be determined, because only one 2D seismic line was available.

(3) Edge Proximity

The distance between the edge of a Z3 stringer and drilling location within that stringer could be determined for thirty-one flowing and six non-flowing Z3 stringer penetrations. The length is specified as the shortest lateral distance—i.e., parallel to the bedding—to the edge. These distances were subdivided into three classes, namely <300 m, 300–1000 m and 1 km. Subsequently, these three classes were labelled as 'Edge', 'Near Edge' and 'Centre' respectively. 77% of the malign stringers were penetrated within 300 m of their edge. Comparably, 50% of the benign stringers were drilled near the edge. Nine flowing and three non-flowing Z3 stringers were left out of the statistics because of T–D relation and seismic quality being too poor and visibility too low. In the case of the non-flowing Z3 stringer penetrated by well TUM-01, the edge proximity could not be determined, because only one 2D seismic line was available.

(4) Relative Depth

The depth of the Z3 stringer relative to top and base Zechstein was determined for thirty-five stringers, in which a value of 0 represents a stringer at top ZE and a value of 1 represents a stringer that forms base ZE. Wells that did not reach base ZE form the set of five stringers not analysed. The relative depths range from a low of 0.06 in URE-202 to a high of 0.88 in F10-03. Since the Z3 stringer is thought to have had an original stratigraphic position in the upper third of the ZE, the reasonable assumption is made that all stringers above 0.4 in relative depth should be close to their original position. The result is that twenty-two stringers fall within the upper category of <0.4 relative depth, which translates to 63% of the total analysed. This suggests the remaining stringers have shifted from their original stratigraphic position. Since the mTVDss of the gain event in a Z3 stringer is used, the relative depth of non-flowing Z3 stringers could not be calculated.

(5) Dip

The highest dip angle of a Z3 stringer at the location of penetration was measured and subdivided into four groups, labelled as 'Horizontal', 'Near Horizontal', 'Dipping' and 'Steep'. These groups correspond to angles in the range of 0–5°, 5–20°, 20–45° and 45–90° respectively. The local dip of a stringer could be determined for thirty-five flowing and seven non-flowing stringers. Respectively 66 and 71% of flowing and non-flowing Z3 stringers had a dip angle below 20°. Three flowing Z3 stringers and one non-flowing Z3 stringer had a dip angle of 45° or higher. The dip angle could not be determined for five flowing and 2 non-flowing stringers, because of a too poor T–D relation, seismic quality or too low visibility.

(6) Shape

A set of thirty-one flowing Z3 stringers was inspected and showed that 58% of kicks occurred when drilling an antiform and another substantial 35% of gains took place when drilling a limb. Conversely, only 1 out of 6 inspected non-flowing stringers penetrated an antiform and 2 out of 6 a limb. Nine malign and three benign Z3 stringers could not be accurately described because of low visibility, poor seismic quality and T–D relation, and were therefore deemed inconclusive.

From the data described above, the assumption arises that drilling an anticline, edge or low-continuity stringer raises the probability of encountering a kick. The percentage of investigated malign Z3 stringers that meet at least 1 of 3 criteria mentioned above amounts to 100%, compared to 50% for benign stringers.

Seismic Expressions

Flowing Z3 Stringers

Total amount of flowing Z3 stringers analysed			**40**
	Classification	**Amount**	
Visibility	Visible	31	
	Invisible	5	
	Inconclusive		4
Continuity	Low Continuity	22	
	Medium Continuity	7	
	High Continuity	1	
	Inconclusive		10
Edge Proximity	Edge	24	
	Near Edge	7	
	Centre	0	
	Inconclusive		9
Depth	Relative Depth <0.4	22	
	Relative Depth >0.4	13	
	Inconclusive		5
Dip	Horizontal	5	
	Near Horizontal	18	
	Dipping	9	
	Steep	3	
	Inconclusive		5
Shape	Anticline	18	
	Limb	11	
	Syncline	2	
	Inconclusive		9

Non-flowing Z3 Stringers

Total amount of non-flowing Z3 stringers analysed			**9**
	Classification	**Amount**	
Visibility	Visible	7	
	Invisible	1	
	Inconclusive		1
Continuity	Low Continuity	1	
	Medium Continuity	2	
	High Continuity	3	
	Inconclusive		3
Edge Proximity	Edge	3	
	Near Edge	2	
	Centre	1	
	Inconclusive		3
Depth			
Dip	Horizontal	2	
	Near Horizontal	3	
	Dipping	1	
	Steep	1	
	Inconclusive		2
Shape	Anticline	1	
	Limb	2	
	Syncline	3	
	Inconclusive		3

Table 1 Summary of the characterization of seismic expressions of flowing and non-flowing Z3 stringers.

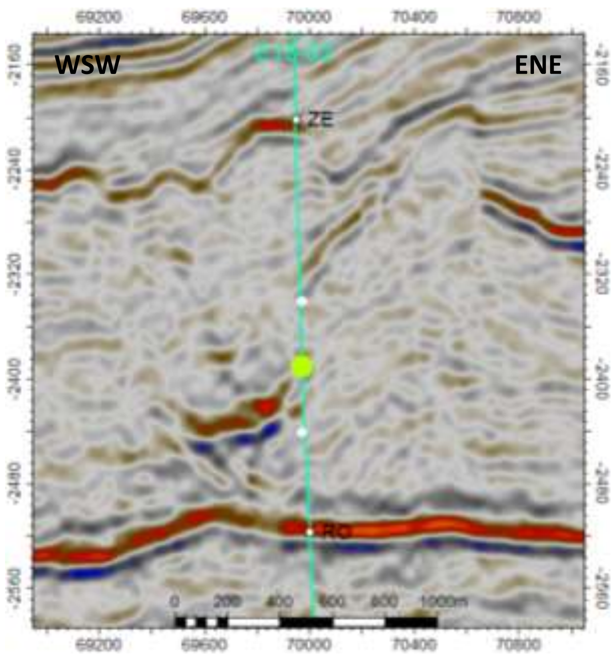

Fig. 3.2*a* Seismic cross-section showing the location at which a kick occurred. Well E18-02 drilled 77 m of Z3 stringer, which is too steeply dipping to be resolved on seismic.

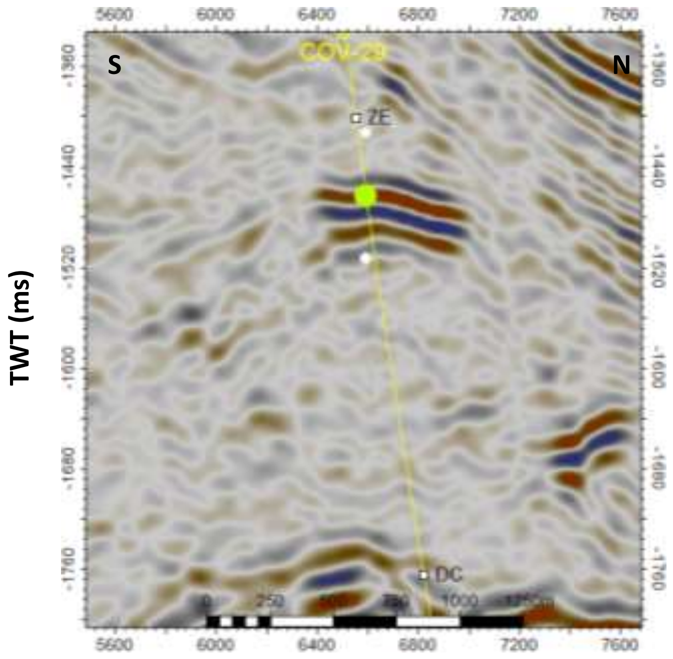

Fig. 3.2*b* Seismic cross-section showing well COV-29 drilled a small-sized Z3 stringer, upon which an influx was taken.

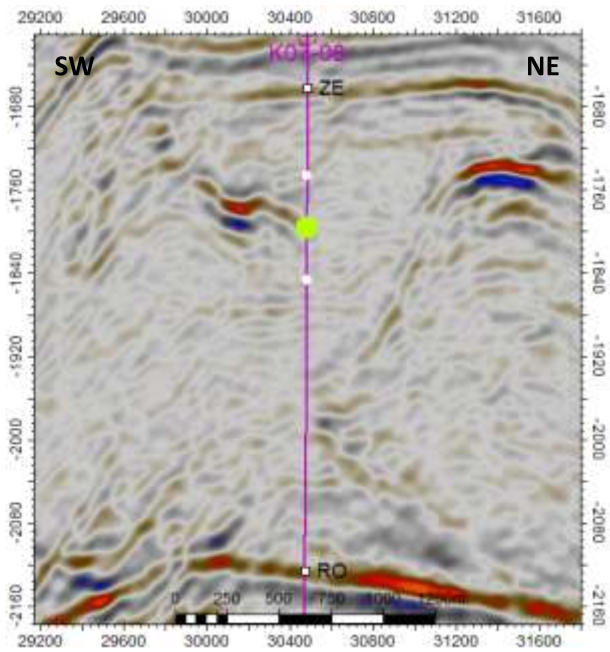

Fig. 3.2*c* Seismic cross-section showing well K07-08 drilled the edge of a Z3 stringer and subsequently experienced a gain event.

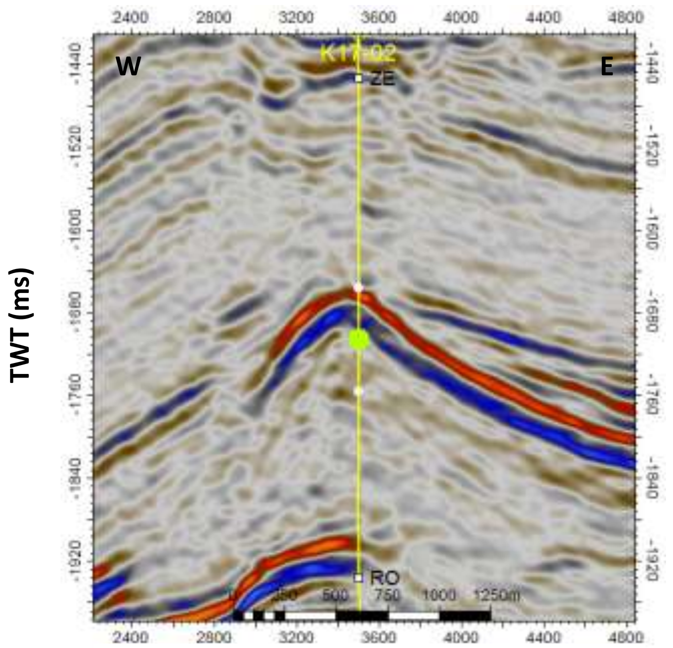

Fig. 3.2*d* Seismic cross-section showing well K17-02 drilled a convex-shaped Z3 stringer which was found to be highly overpressured.

□ Well Top

● Kick

○ 50 ms Uncertainty

Fig. 3.2 Seismic is in time domain with 5x vertical exaggeration.
Red loops represent an acoustic hardening.
x-axes represent either Inlines or Xlines with a seismic bin size of 25 m.

3.3 Pressures

Stress gradients represent the increase in applied stress with increasing depth. In case of the lithostatic gradient (vertical stress, σ_v), the stress at a certain depth equals the product of the density, the total height of the rock column and the gravitational force. The gradient is therefore dependent on the density of the overburden, which in turn is dependent on lithology, porosity and fluid content of the pores. In the literature, lithostatic gradients for sedimentary basins are commonly displayed as linear lines with a gradient that ranges from 2.0 to 2.3 bar/10 m (e.g. **Gaarenstroom et al., 1993; Kukla et al., 2011; Zijp et al., 2018**). **Fig 3.3*a*** contains five lithostatic stress gradients of Dutch wells for which near-complete density logs are available. In addition, the theoretical lower- and upper limit of 2.0 and 2.3 bar/10 m are plotted, as well as gradients for water and quartz (with 0–10–20–30% porosities). The figure shows that although lithostatic gradients cannot be represented by linear lines in reality, the two theoretical constraints of 2.0 and 2.3 bar/10 m do capture the maximum deviation for a large part. At shallow depths the wells seem to lie on or below the lower limit and are more or less parallel to the quartz gradient with 30% porosity. The gradient for the onshore well seems to increase from ~600 m, whereas the offshore wells show a similar trend from ~1300 m onwards. From here they resemble the pressure gradient for quartz with a 10% porosity. In the offshore wells the gradient stays below the upper limit, whereas the pressure of the onshore well exceeds this boundary from 1600 m onward.

Zechstein pore pressures have been plotted versus mTVDss (**Fig. 3.3*b***), in order to get a better overview of overpressures in the ZE and to test the statements of **Hoetz (2018)**. A total of sixty-six ZE pressures were derived from the kill mud weight (in s.g.). These points represent the maximum pore pressure as recorded in the borehole, plotted against mTVDss. Included are the hydrostatic and theoretical lower- and upper limit lithostatic gradients described above. Triangles, squares and circles represent carbonate, anhydrite and halite lithologies respectively. Gold, blue, grey, orange and green colours represent Z4, Z3, Z2, Z1 formations and undifferentiated ZE respectively. The figure illustrates that pore pressures increase with depth and most points plot near the lithostatic gradients. Two points even plot above the theoretical upper limit of 2.3 bar/10m, namely the kicks encountered in wells COV-29 and ENA-02. Carbonate lithologies are more prone to hard overpressures than anhydrite and halite. Fifty-six percent of the kicks from carbonate members were above 2.0 s.g., compared to thirty percent for both anhydrite and halite members.

The distance in mTVD between the depth of top ZE and the gain has been plotted in **Fig. 3.3*c***. Included are the hydrostatic and lithostatic (2.3 bar/10 m). Symbol type and colour follow the same convention as in **Fig. 3.3*b***. The figure shows the amount of ZE (in mTVD) that overlies the point at which the kick was taken, plotted against the specific gravity of the mud weight. The gains encountered in wells F04-03 and F07-02 illustrate that respectively only 42 and 46 m of overlying ZE is needed to create pressures above 2.1 s.g. Furthermore, the 0 m distance of F10-02 suggests no overlying ZE salt is needed at all to create pressures of 2.0 s.g. Pressures above 2.1 s.g. seem most prevalent in the 0–600 m range distance between gain and top ZE.

Fig. 3.3 *a*) Dashed lines illustrate hydrostatic gradient of 1.0 bar/10 m, theoretical lithostatic gradients of 2.0 bar/10 m and 2.3 bar/10 m, quartz gradient of 2.7 bar/10 m and quartz gradients with 10, 20 and 30% porosity. Integration of density logs of five Dutch wells representative for lithostatic gradient in Netherlands. mTVDss represents true vertical depth with respect to subsea in metres and is plotted versus pressure in bar. ***b***) Measured kill mud weight data converted to pressure. Colours and symbols represent respectively the ZE stratigraphic group and lithology from which a kick originated. Hydrostatic gradient of 1.0 bar/10 m, theoretical lithostatic gradients of 2.0 bar/10 m and 2.3 bar/10 m. mTVDss represents the true vertical depth of kicks in metres with respect to subsea and are plotted versus pressure in bar. ***c***) Measured kill mud weight data plotted versus distance between top ZE and depth of kick in metres true vertical depth. Colours and symbols of points represent respectively the ZE stratigraphic group and lithology from which a kick originated. Hydrostatic of 2.0 s.g. (specific gravity) and lithostatic of 2.3 s.g.

Fig. 3.3*a*

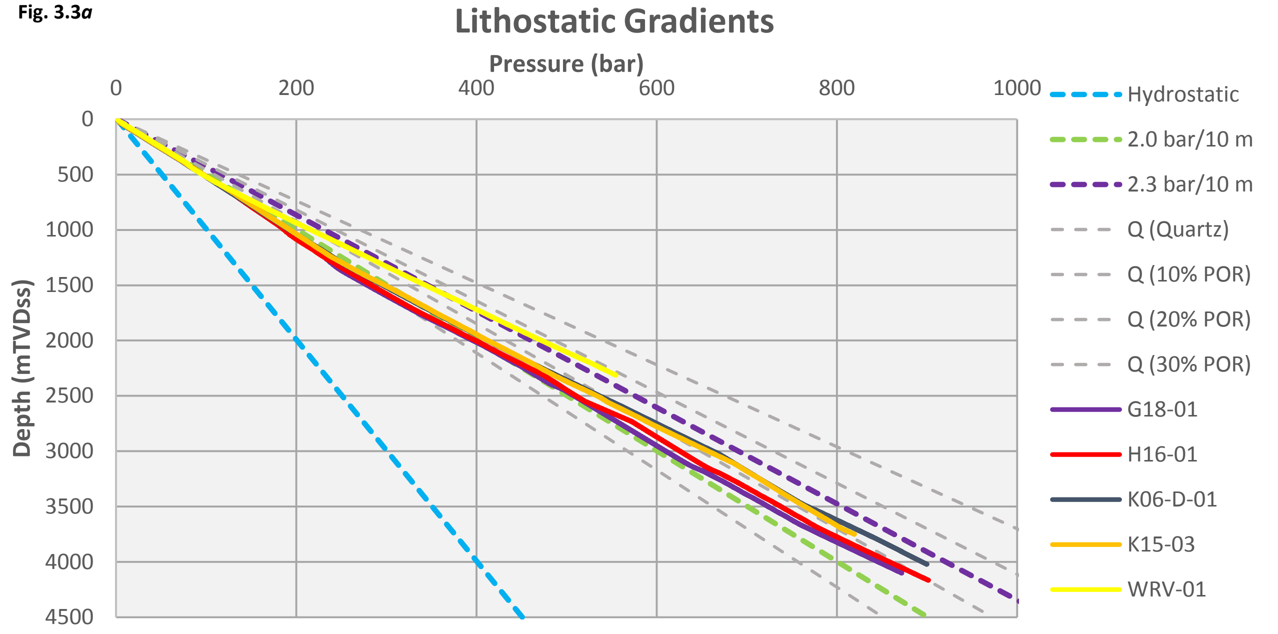

Fig. 3.3*b*

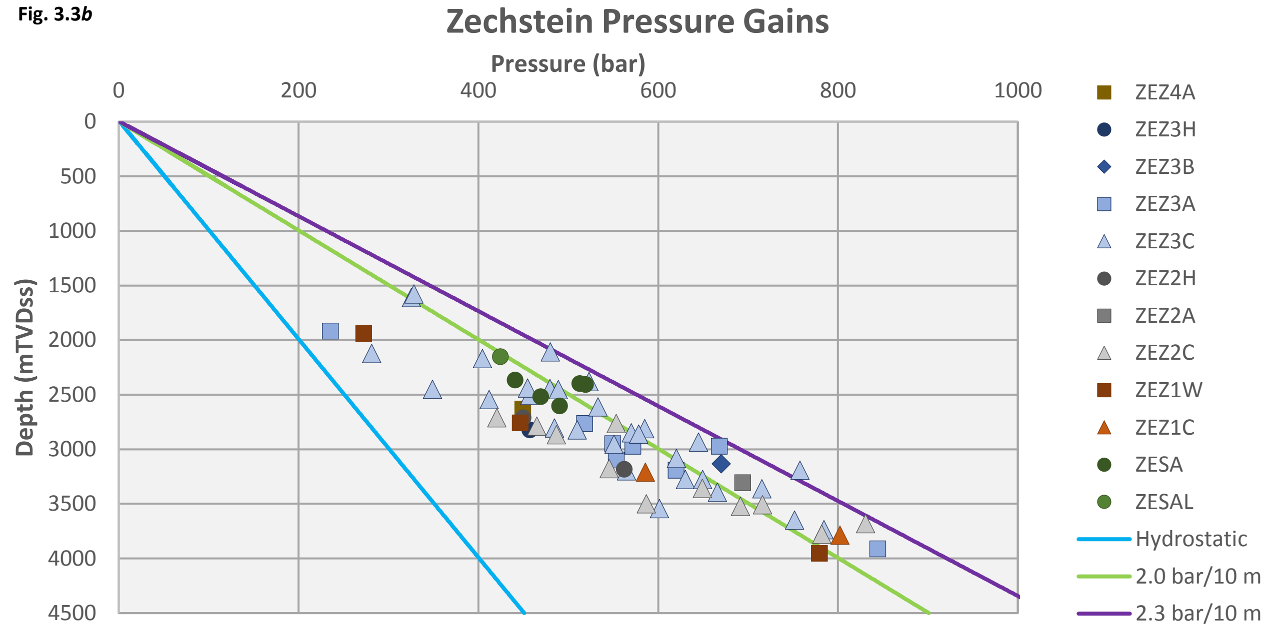

Fig. 3.3*c*

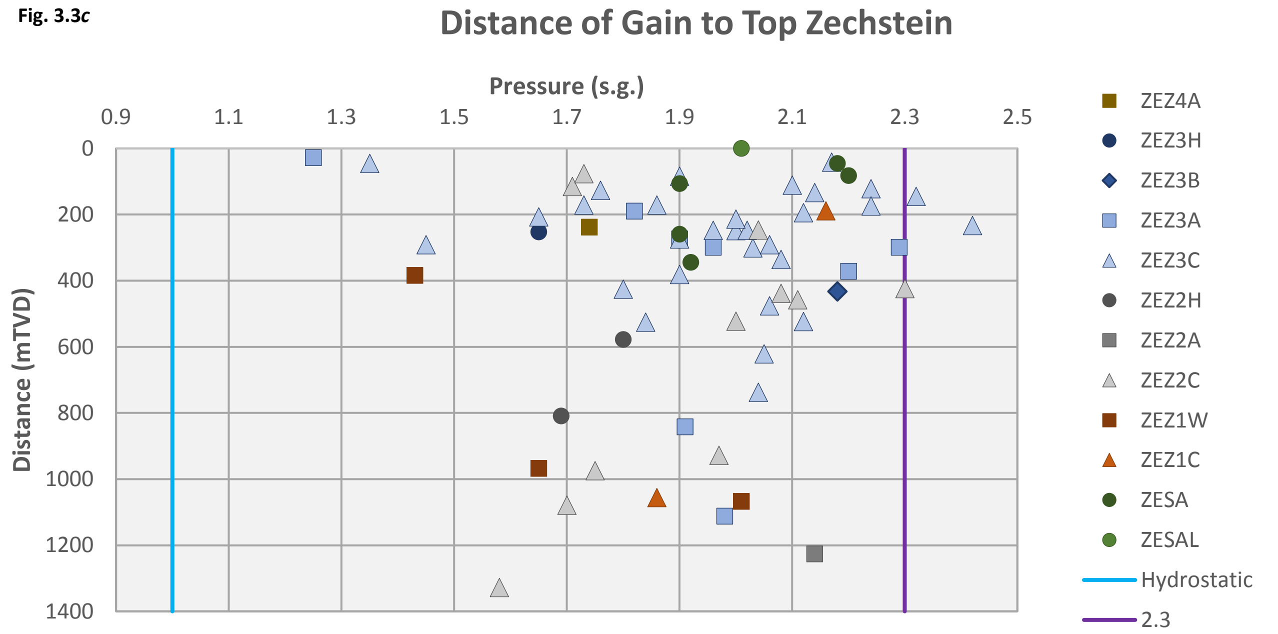

4. Discussion

The data presented in the previous chapter can be integrated to represent a model for the prediction of overpressures in Z3 stringers based on seismic expressions. Firstly, it must be established which overpressure mechanisms take place in the ZE. In order to do this, it is important to determine the magnitude of the principal stresses in the Dutch subsurface, which control the boundaries of pore pressures. In addition to overpressure mechanisms and their magnitudes, the fracture distribution within the different ZE members must be considered. Secondly, the ZE overpressures are correlated with seismic expressions to establish a model that constrains the probability of taking a kick when drilling certain Z3 stringer configurations.

4.1 Overpressure Mechanisms

4.1.1 Lithostatic Stresses

The Netherlands is characterised by a normal faulting regime and as a result, σ_v is the maximum principal stress. This means stresses within the Dutch subsurface are dictated by σ_v, which in turn is governed by the weight of overlying rock for each point in the subsurface. **Fig. 3.3*a*** shows that due to the fact that rock density tends to increase as a function of depth, lithostatic gradients cannot be represented by linear lines in reality, the two theoretical constraints of 2.0 and 2.3 bar/10 m do capture the maximum deviation of lithostatic gradients in the Netherlands for a large part, based on the five wells that were analysed in this study. At shallow depths the wells seem to lie on or below the lower limit. One explanation for this observation is that the shallow—mainly siliciclastic—sediments have not undergone significant compaction. Hence, they have relatively high porosities, resulting in densities below 2.0 s.g. This is reflected by the gradient of quartz with 30% porosity. The gradient for the onshore well seems to increase from ~600 m, whereas the offshore wells show a similar trend from ~1000 m onwards. This is explained by the fact that the onshore well encountered the Chalk Group at much shallower depth than the offshore wells (**Table 2**). In the offshore wells the gradient stays below the upper limit, whereas the vertical stresses of the onshore well exceeds it from 1600 m onward. Since WRV-01 is located on the southern edge of the Southern Permian Basin it encountered fringe clastics instead of evaporites. The offshore wells encountered >474 m of halite (**Table 2**), which has a density of only 2.1 s.g. This could explain why only the onshore well exceeds expected vertical stresses. In addition, wells drilled after 1980 commonly have a non-vertical component in their trajectory. This implicates that there is an uncertainty in positioning and deviation of a borehole. Density is measured along a borehole and when the positioning and deviation are off this results in density values correlated to incorrect true vertical depths. Furthermore, sedimentary layers are not always horizontal—be it the result of depositional- or tectonic processes. The thickness of a certain stratigraphy as encountered by a (deviated) well is determined by the relation between the top and base of the interval and the angle at which it was drilled. The angle at which a well was drilled with respect to the dip of the stratigraphic layer is not taken into account. This effectively means that the thickness of a stratigraphic layer is either determined correctly or overestimated. For example, when a Z3 stringer with a thickness of 50 m is drilled along strike, this could result in encountering >200 m of Z3 stringer. Such was the case with the Dutch onshore well NSN-01. Naturally, this has a big effect on the measured density and therefore on the gradient.

Well	Top CKGR mTVDss	ZE Halite Thickness mTVD
G18-01	1003	888
H16-01	968	670
K06-D-01	1299	474
K15-03	1238	597
WRV-01	569	0

Table 2 Top CKGR and ZE halite thickness as encountered in the five Dutch wells from which density logs were integrated to estimate the lithostatic.

4.1.2 Poroelasticity

In order to properly assess the hard overpressures observed in the Zechstein, it is necessary to discern which overpressure mechanisms control the pore pressure in the ZE. The following sections deal with the first mechanism: disequilibrium compaction. In order to understand this mechanism, it is important to understand the theory of poroelasticity, which describes the relation between stress matrix and bulk strain matrix, as well as the pore pressure and pore strain. These stresses and strains are coupled in the sense that the bulk strain is affected by the pore pressure (**Zimmerman, 1991**).

Under slow deformation conditions rock salt behaves incompressibly (non-dilatant). In this non-dilatant viscoplastic strain rate regime, the Poisson's ratio of rock salt is essentially 0.5; almost an ideal plastic deformation condition with a zero plasticity angle (**Liang et al., 2011**). Comparably, the Poisson's ratio for anhydrite, carbonate and shale are about 0.25 (**Liang et al., 2007**), 0.3 (**Kłeczek, 2016**) and 0.3 (**Sone, 2012**) respectively. The consequence of a Poisson ratio of 0.5 is that all shear stresses vanish and (normal) stresses within salt bodies become uniformly equal to lithostatic. **Eq. (1)** by **Eaton (1969)** illustrates that with a Poisson ratio of 0.5, σ_h will equal σ_v:

$$\sigma_h = \frac{v}{1-v}(\sigma_v - p) + p \qquad (1)$$

where σ_h is the minimum horizontal stress; v is Poisson's ratio; σ_v is the vertical stress and p is pore pressure. This suggests that only normal stresses—of equal magnitude—are applied to a completely isolated Z3 stringer, even though the lithologies that make up a stringer have lower Poisson ratios. Since the principal stresses applied to a stringer are all equal, there is no deviatoric or 'effective' stress and hence, no fractures will be created. **Skempton (1954)** showed with the *B*-coefficient (**Eq. 2**) that when a compressive stress is applied to a small volume of saturated porous material surrounded by an impermeable boundary, the induced pore pressure is *B* times the applied stress. Note that the total sum of applied stresses to the system is described with $\sigma_h = \sigma_H = \sigma_v$.

$$B = \frac{\Delta p}{\Delta \bar{\sigma}} = \frac{\frac{K_f}{\varphi}(1 - \frac{K_{fr}}{K_s})}{\frac{K_f}{\varphi}\left(1 - \frac{K_{fr}}{K_s}\right) + K_{fr}(1 - \frac{K_f}{K_s})} \qquad (2)$$

where *B* is the Skempton coefficient; Δp is the difference in pore pressure; $\Delta\bar{\sigma}$ is the difference in mean principal stresses; K_f is water compressibility; K_s is rock compressibility; K_{fr} is bulk compressibility and φ is the porosity. *B* must lie between 0 and 1 and is a measure of how the applied stress is distributed between the matrix and fluid respectively. The equation illustrates that if the porosity is low and the bulk modulus (K_{fr}) high, *B* will be low and consequently, much of the stress is applied to the matrix. Thus, when drilling an unfractured stringer, which is shown to have a high bulk modulus, no hard overpressures are expected. If a Z3 stringer is highly fractured, the porosity increases moderately, whereas the bulk modulus decreases significantly. In this case *B* will approach 1 and as a consequence much of the stress will be applied to the pores. If permeability is sufficient, it is expected that pore pressures are close to lithostatic. Thus, it is crucial to understand the initiation and distribution of fractures—particularly in the carbonate members—in order to better predict the porosity and permeability of Z3 stringers and the ZE in general, and therefore the magnitude of overpressures.

4.1.3 Concept of Fracture Gradient

Fracture pressure is the pressure required to fracture a formation and to cause mud losses from a wellbore into the induced fractures. The *fracture gradient* is obtained by dividing the TVD with the fracture pressure (**Zhang & Yin, 2018**). The minimum horizontal stress (σ_h) is very critical for fracture gradient prediction and is commonly estimated from downhole tests, such as leak-off tests (LOT, **Fig. 4.1.2**). However, LOT data normally are not available at the location and depth of interest (**Zhang & Zhang, 2017**). The challenge is to accurately determine the fracture gradient, which is dependent on overburden stress, pore pressure, depth (**Zhang & Yin, 2018**) and lithology (**Zhang & Zhang, 2017**), and may range from the fracture closure pressure (i.e., σ_h) to the formation breakdown pressure (**Gaarenstroom et al., 1993; Zhang & Yin, 2018**).

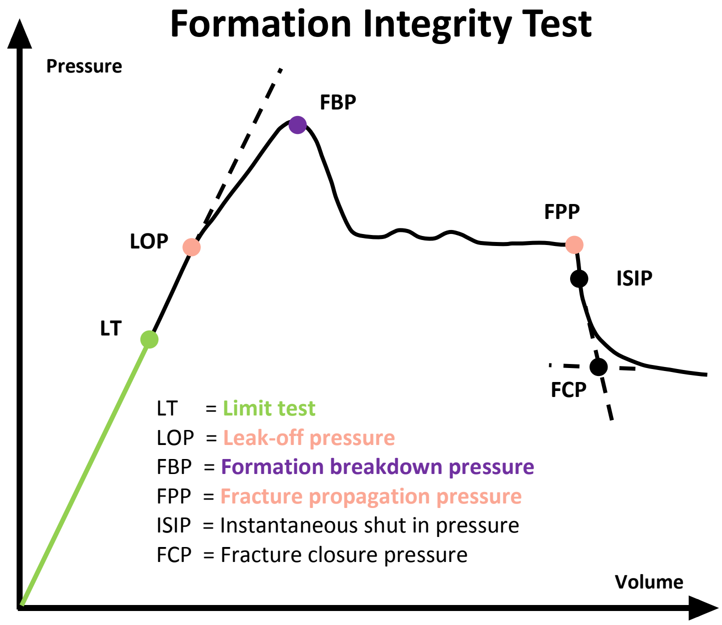

Fig. 4.2 Pressure and stress nomenclature *modified after* ***Gaarenstroom et al., 1993***.

4.1.4 Fracture Distribution

The distribution of fractures within a volume of rock is controlled by several factors including stratigraphy, diagenesis and structural parameters; relations to faults and folds and tectonic history. The connectivity of a fracture network is dependent on the orientations, size distribution and densities of the different fracture sets. Carbonates are commonly very heterogeneous with respect to both matrix and fracture properties. Heterogeneities are caused by fracturing at different scales superimposed on inherent heterogeneous textures from deposition and diagenesis. Furthermore, carbonate rocks are highly chemical reactive; dissolution, cementation and dolomitization processes may affect the reservoir properties at any time during deposition, burial or subsequent exhumation (**Wennberg et al., 2016** ***and references therein***).

Diagenetic processes that cause carbonate rocks to become brittle initiate shortly after deposition. Brittle deformation tends to involve dilation, with space being created by fractures. Fault damage zones are locations at which there is a major change in fabric, or are areas of fracturing around and related to a fault. Such zones are typically created by fault propagation, linkage or displacement along the fault. Knowledge of damage zones enables predictions of dilation areas, and, therefore, the enhanced fracture porosity and permeability along and around fault zones. Larger faults on the other hand, may form conduit–barrier systems to fluid flow, in which parts of a fault may represent a barrier to fluid flow due to cataclasis and cementation in the fault core, and other parts represent a conduit due to fracturing in the damage zone. (**Wennberg et al., 2016** ***and references therein***). In addition, higher fracture frequencies in areas of maximum curvature indicate that folding controls fracture frequencies (**Peacock & Mann, 2005**), due to flexural stretching.

The distribution of porosity and permeability in the ZEZ3C is controlled by the depositional facies and diagenesis (**Brooks et al., 1986**). On average, the porosity and permeability show a range of 2–5% and 1–10 mD respectively. The uppermost part of the formation can exhibit higher porosities and permeabilities—up to 10% and 400 mD respectively—as a result of leaching that occurred during aerial exposure. Conversely, undeformed anhydrite cores of the ZEZ1W show connected porosities of 0.1–0.3% and permeabilities below the detection limit (**Hangx et al., 2009**). Similarly, compaction and cementation lead to nearly zero porosity in rock salt below a burial depth of 30 m (**Kukla et al., 2011**). Shale, although having typical porosities in the range 1–5%, has very low permeabilities (**Liu, 2015**).

Thus, it is expected that after deposition, anhydrite, halite and shale exhibit a much lower porosity and permeability distribution compared to carbonate. The fracture frequency in anhydrite, shale and carbonate may increase near faults or fold hinges, as these lithologies tend to display brittle failure, whereas salt tends creep during deformation. Particularly in carbonates, these newly created fractures could connect with the initial fracture network to form a permeable zone. This will significantly lower the bulk compressibility (K_{fr}) and from **Eq. 2** it follows that Skempton's coefficient *B* will approach 1, meaning that most of the stress will be applied to the pores. When drilled, pore pressures close to lithostatic will be encountered.

Log data in wells E18-02, F10-03, G18-01, COV-29, COV-48-S2 and GSV-01 show evidence of increased permeability in carbonates. A common thread in the data (if available) is an increase in P-sonic time, decrease in density and increased neutron-, resistivity- and caliper readings at a flowing zone.

The same mechanism as described above could also create fractures in halite. Lab experiments yield Poisson ratios of 0.31 for halite (**Liang et al., 2007; Jackson & Hudec, 2017**). This indicates that when strain rates are sufficiently high, shear stresses may exist and halite will break. As a result, for example, **Fredrich et al. (2003)** found that some of the drilling problems encountered when drilling through the bottom of a salt structure, that are usually attributed to very weak rock in a hypothesized rubble-zone, may actually be associated with concentrated deviatoric stresses at the bottom of the salt body.

The discussion above describes how overpressures in the ZE may be generated, purely due to effective isolation of fractured Z3 stringers. However, data obtained in this research show evidence of a second overpressure mechanism; fluid expansion as a result of gas generation. The following section deals with this topic.

4.1.5 Fluid Expansion

Gases were observed in 40% of the kicks that occurred in the ZE. This suggests gas generation may form an important overpressure mechanism in the ZE. The most likely formations with source rock potential are the carbonate members of the ZE (**Brooks et al., 1986; Geluk, 2000**) and Westphalian coals. Indeed, 77% of gas kicks were encountered in ZE carbonate members. However, six gas kicks originated from halite and anhydrite members.

Halite—and anhydrite to a lesser extent—is considered to be a perfect seal (**Downey, 1984**) and therefore, it seems unlikely that gas kicks can take place within rock salt. However, black stains and hydrocarbons have been observed above stringer intervals in salt cores retrieved from the Aral salt of Oman (**Kukla et al., 2011**). These halite samples were found to contain bands with µm-sized oil and gas inclusions, alternated by thin, fluid inclusion-free bands. They also showed evidence for crystal plastic deformation and dynamic recrystallization. The proposed mechanism that leads to fluid migration in halite involves pressures high enough to open grain boundaries, allowing brines in pore throats of salt to be displaced, causing a diffuse dilatancy (**Kukla et al., 2011**). Halite has a low interconnected porosity represented by a triangular space between grains. If σ_h of halite is exceeded by the capillary entry pressure, a fluid is allowed into the triple junction tubes of the salt, leading to a diffuse dilation of halite by grain boundary opening and intragranular microcracking. As a result, permeability increases by orders of magnitude (**Kukla et al., 2011**) and so-called brine or gas pockets may form within halite members. To illustrate, a gas kick occurred in well F07-02 within halite above a Z3 stringer in an anticlinal structure. The most likely source of this gas is the underlying Z3 stringer. Apparently, cracking of kerogen into gas within the ZEZ3C generated enough overpressure to breach the overlying rock and to accumulate in overlying halite in a gas pocket. Skempton's coefficient *B* shows brine or gas pockets may yield pore pressures close to lithostatic as a result of increased permeability. If overpressure generation persists then fractures may propagate further upward in the formation and form so-called *fluid migration paths*. Evidence for such paths is given on seismic in **Appendix C** and will be further discussed in section **4.2.3**.

Some of the ZE gains may be related to shales. Wells AME-205, TVN-01 and perhaps LWZ-03-S1 drilled a section of shale, after which a sudden influx occurred. **Hoetz et al., (2013)** propose the concept of a shale-capped brine chamber, in which brines percolating up through salt become trapped by shales. The proposed mechanism involves dehydration of halite upon compaction. Brine migrates upwards due to pressure dissolution and/or micro-fracking and is arrested at a non-soluble layer, such as a shale. If this shale forms a closure, then brine may accumulate. Seismic shows an anticlinal structure at the location AME-205 experienced the kick, which could be related to a shale-capped brine chamber (**Appendix C**). It is widely accepted that halite and anhydrite form a better seal than shale (**Downey, 1984**). However, under suitable conditions all rocks can lose their sealing capacity, and the geological conditions for seal loss of rock salt are not well understood (**Schoenherr et al., 2007**). Therefore, conditions might exist under which shales have a higher fracture propagation pressure than halite. Alternatively, shales may have source rock potential and generate their own overpressures. Shales are less ductile than rock salt and may break during deformation, resulting in increased permeability.

Based on the above discussion it is assumed that the majority of overpressures in the ZE are generated through disequilibrium compaction. Gas kicks mainly originated from carbonate and perhaps shale lithologies. The main overpressure mechanism in this case is through gas generation and effective sealing. Gas kicks in anhydrite and halite lithologies are probably linked to overpressures in underlying carbonates. In the following sections, an attempt is made to link the magnitude of overpressures to stratigraphic members, in order to further assess the origin of overpressures within the ZE.

4.1.6 Zechstein Overpressures

As discussed in the previous sections, overpressures in the ZE are thought to be established through either gas generation—irrespective of whether the source rocks were ZE carbonates and shales or formations in the underburden—and effective sealing of these pressures or through intense fracturing of isolated stringers, lowering the bulk modulus, which, according to Skempton's coefficient *B*, transfers most of the applied stresses to the pores.

The ZE kicks obtained in this study show a depth-related trend and most plot near the lithostatic. (**Fig. 3.3*b***). Based on the stratigraphic member in which they occurred, kick events are divided into the following groups *(1)* Basal ZE, *(2)* Z3 Stringer, *(3)* Rock Salt and *(4)* Inconclusive. Inconclusive in this case means it could not be determined from which ZE member a kick originated.

(1) Basal ZE

Although the basal ZE members are mechanically coupled to the underburden, the ZEZ1W and ZEZ2A are assumed to be isolating. Indeed, H_2S in the ZEZ2C has never migrated through the ZEZ1W into the RO during production (**Martin Ecclestone, personal communication, 2019**). This means that up to ZEZ1W the basal ZE is assumed to be in connection with the underburden. The most likely overpressure mechanism in these stratigraphic members is through the generation of gas and effective sealing by overlying halite. Indeed, gases were observed in 76% of the basal ZE kicks. The average pressure of brine kicks was 2.10 s.g. compared to a pressure of 1.83 s.g. from gas kicks. This can be explained by the fact that gas has a much higher compressibility than brine. From **Eq. 2** it follows that more stress will be applied to brine-filled pores compared to gas-filled pores.

It is assumed that hydrocarbons generated in the ZEZ1K and ZEZ1C will migrate downward into the RO. As a result, no hard overpressures are expected in the ZEZ1C. However, in certain areas the Ten Boer Claystone forms top RO, which is isolating. In this case the hydrocarbons generated in the ZEZ1C and ZEZ1K are trapped and hard overpressures will be created. As expected, wells K07-08 and L08-H-02-S1 encountered a kick in the ZEZ1C that was underlain by the impermeable Ten Boer Member. All three kicks that originated from the ZEZ1W were related to gases. These gases could have originated from the ZEZ1K and ZEZ1C in case the Ten Boer Member isolated the RO from the ZE, from dolomite stringers within the ZEZ1W itself (see section **4.1.9**) or from overlying ZEZ2C. An important finding is that only Z1 anhydrite immediately overlying ZEZ1C is found to be overpressured. The Z1 Upper Anhydrite Member (ZEZ1T, separated from the ZEZ1C–ZEZ1A succession by halite of the ZEZ1H) is not found to be overpressured. All onshore ZEZ2C kicks contained gases, suggesting that the ZEZ2C has proper source rock potential. On average, gains encountered in the *Z1 (Werra) Formation* have a lower pressure than kicks taken in the *Z2 (Stassfurt) Formation* (1.82 vs. 1.93 s.g.). In all cases of ZEZ2A/C gains, no ZEZ1H was encountered to separate the Z1 and Z2 formations. Apparently, ZEZ2C is unable to withstand high overpressures (>2.0), whereas ZEZ2H overlying the ZEZ2A/C forms a seal that is competent enough to withstand these high overpressures.

(2) Z3 Stringer

Forty-five kicks occurred in stratigraphic members overlying the basal ZE, of which forty took place in Z3 stringers. Twenty-nine of these stringers took a brine influx. It could be determined from seismic and well data that the stringers penetrated by wells GRO-01, URE-202 and VRS-401 were connected to the over- or underburden (**Appendix C**). Consequently, the average pressure as observed in these three wells was 1.35 s.g., which is regarded as a soft overpressure (**Loucks et al., 1979**). The average brine kick pressure of the isolated Z3 stringers was 2.04 s.g., which is higher compared to the pressure of the gas kicks encountered in eleven isolated Z3 stringers, which was about 1.98 s.g. This difference is probably the result of the higher compressibility of gas. From **Eq. 2** it follows that more stress will be applied to brine-filled pores compared to gas-filled pores. Brine kick pressures measured in the ZEZ3C penetrated by COV-29 and ENA-02 even exceed the theoretical lithostatic limit of 2.3 bar/10 m. The lithostatic gradient of well WRV-01 as displayed in Fig. 3.3.1 shows this is possible. It is worth noting that these three wells were all drilled onshore and probably have a higher gradient because of conditions described in section 4.1.1.

(3) Rock Salt

Respectively three and one brine kicks originated from the ZEZ2H and ZEZ3H members and are known as so-called brine pockets. No gas kicks were related to halite members. Kick pressure data was available for 3 out of 4 events and had an average of 1.74 s.g. Assuming these brine pockets are surrounded by impermeable salt, it is expected that the total sum of normal stresses acting on the bulk (rock and fluid) is equal to the vertical stress in all directions, while shear stresses vanish. The ratio of stress applied to fluid versus solid in halite is apparently lower compared to that of anhydrite and carbonate.

(4) Inconclusive

In six cases it could not be determined from which ZE member a kick originated. Two of these kick events were related to gases, with an average kick pressure of 2.10 s.g. The remaining four cases observed a kick pressure of 1.98. These pressures indicate it is more likely these kicks were related to anhydrite or carbonate members than to halite. Boreholes L04-PN-04 and L04-PN-04-S1 experienced brine kicks in the 'Zechstein Group' according to NLOG. The drop in ROP, increase in GR and seismic reflectivity indicate this could be a Z3 stringer, but seismic quality and T–D relation are too poor to be conclusive.

On average, carbonate lithologies are more prone to exhibit hard overpressures than anhydrite and halite lithologies, even though most gas kicks are associated with carbonates. Carbonates are known to fracture shortly after deposition. Therefore, the fracture frequency in deformed carbonates is thought to be higher, relative to anhydrite and halite experiencing the same magnitude of deformation. This greatly diminishes the bulk modulus of carbonate and as a result relatively more stress will be applied to the pores, perceived as higher kick pressures. On average, isolated Z3 stringers contain higher pore pressures than basal ZE members (2.02 vs. 1.90 s.g. respectively). The main mechanism generating overpressure in Z3 stringers is disequilibrium compaction, whereas fluid expansion through maturation of kerogen into gas is the main overpressure mechanism in the basal ZE. The overpressures described above will be linked to seismic expressions in section **4.2**. The following section deals with uncertainty in the magnitude of overpressures.

4.1.7 Uncertainty in Magnitude of Overpressures

The points in **Fig. 3.3*b*** should reflect the maximum pore pressure as recorded in the borehole, plotted against mTVDss. However, these points must be considered in context of their uncertainty. Ideally, pore pressures are measured with wireline tools, such as the repeat formation tester (RFT) or formation micro tester (FMT) tools. Unfortunately, these tests are generally not carried out on the formation of interest for this study. It is therefore decided to rely on mud weight data. Pore pressures plotted in **Fig. 3.3*b*** are derived from the mud weight used to kill the well. When this 'overkill' mud weight is converted to pressure, it will give an overestimation of the pore pressure. A more in-depth discussion of this topic is described in section **4.2.2**.

This overestimation was likely the case for the gains encountered in boreholes D15-04, E17-02, F04-03, F07-02, F10-03, G18-01, GGT-103, GTV-01-S1, K07-07, K07-07-S2, K07-08, K07-13, K08-FA-307, K08-FA-308-S1, K09AB-B-03-S1, K10-17, K11-FA-103, K15-11, L08-H-02-S1 and MKZ-06. In all cases the mud was weighted up to a point where it induced losses. What's more, after weighting up the mud, well K11-FA-103 experienced losses which reduced and turned into gains—indicating recharging of the producing zone. This suggests the chosen mud weight was so high that the fracture propagation pressure was exceeded upon which new fractures were created, thereby increasing the connected volume. Reversed bias may occur when a connected volume is sufficiently small. When a well has already seen inflow, the total volume of formation fluids has effectively been lowered and therefore the mud weight used to kill the well is not required to be as high as when the total volume would still be in place.

4.1.8 Distance of Gain to Top Zechstein

It is general practice to set casing in Top ZE for the dual purpose of ensuring the casing is set in a competent layer and to isolate overlying weak formations from unexpected overpressures encountered deeper in the ZE. A recurring point of debate is whether it is safe to drill 'unprotected' into the ZE. Top ZE is not always clearly observable on seismic and it can be difficult to determine the top during the drilling phase. In practice this means that a few metres of ZE may be drilled before it is determined that the ZE has been entered. The depth of Top ZE used in this report is based on NLOG-data. ZEUC forms Top ZE and is present in the entire distribution area of the ZE Group, unless truncated locally by later erosion (**Adrichem-Boogaert & Kouwe, 1994**). It is assumed that a certain amount of halite is needed to retain overpressures over long periods of time (**Kukla et al, 2011**). The ZEUC member consists of mainly clay and should therefore not be taken into account when determining the total thickness of ZE overlying a flowing zone. However, this member is not always defined in the NLOG database and therefore the top of the ZE Group is used in this research. Uncertainty in deviation data may affect the calculated TVD of Top ZE and the depth of a kick. In addition, the depth of a flowing zone might be overestimated, as explained in more detail in section **4.2**.

Fig. 3.3*c* illustrates the thickness of ZE in mTVD overlying the point at which a ZE kick was taken, plotted against pressure gradient (s.g.). The shallowest point represents the gain observed in well F10-02, which was encountered at 0 m below Top ZE. However, NLOG reports 175 m of UNKNOWN stratigraphy above the depth of the kick, meaning that the actual distance between the depth of the kick and Top ZE in this well lies between 0 and 175 m. Therefore, this point should be discarded. URE-202 and GRO-01 encountered a kick at 29 and 46 m below Top ZE respectively. However, in both cases the ZEZ3A/C—from which the kick was taken—directly underlies the ZEUC. No halite is present to isolate the competent layers of the *Z3 (Leine) Formation* from the overburden and consequently they are only mildly overpressured (1.25 and 1.35 s.g. for the influxes taken in URE-202 and GRO-01 respectively). The high-pressure kicks observed in wells F04-03 and F07-02 were encountered at 42 and 46 m below Top ZE respectively. In both cases, NLOG defined ZEUC, and subtracting its thickness from the total thickness of overlying ZE leaves only 30 and 35 m of halite.

Kick pressures above 2.1 s.g. seem most prevalent in the 0–600 m range distance between gain and top ZE. As discussed in section 4.1.6, this is probably related to the fact that kicks that occurred in Z3 stringers had a higher pressure, and the majority of Z3 stringers are positioned in the upper half of the ZE.

The ZE kicks investigated in this report indicate that as little as 30 m of impermeable halite is needed to retain high overpressures. It is important to realize that this number is based on a total of 960 investigated Dutch wells, wherein 68 ZE gains were identified. Since the total amount of wells drilled for E&P purposes in the Netherlands amounts to 5437, it is expected that more ZE gains have occurred, in which the salt overlying an overpressured zone may be even thinner. Indeed, **Zonjee (2018, personal communication)** mentions a case in which only 25 m of overlying halite was found to seal hard overpressures and that as little as 4 m of halite was found to separate hydrostatic pore pressures from near-lithostatic stresses in evaporite basins. (No specific well or basin was mentioned in which this case occurred, due to confidentiality reasons.) The general lack of pressure transitions prior to drilling into a stringer reflect their isolated nature and sharp boundaries within the salt (**Warren, 2016**). To conclude, it is advised not to drill too deep into the ZE unprotected. The next section deals with uncertainties in the depth of kick events and correspondingly the stratigraphic member in which the kick event occurred.

4.1.9 Uncertainties in Depth of Gains

It is common practice that the stratigraphic member last encountered before the well gained is regarded as the one that flowed. For example, an overpressured stringer in which the pores are entirely connected will flow as soon as it is drilled. When this flow cannot be controlled and the well has to be abandoned, then it is mistakenly determined to have come from the overlying stratigraphy. This was likely the case for gains observed in boreholes MKZ-06 and K15-FG-104-S1, which were ascribed to ZEZ3A instead of ZEZ3C.

Formation fluid flows are observed as a rising level of fluids in the trip tanks or trip gas. Detection- and tolerance limits depend on hole size and depth. Drilling mud volumes are smaller and more stable when drilling deep boreholes with small diameters, meaning gains can be detected earlier compared to shallow, large-diameter boreholes. In practice, a gain of a couple of hundred litres forms the lower detection limit (**Lammers, 2018, personal communication**). The lag time between the start of a formation fluid flow and detection can range from anywhere between one minute and a few hours. In case a highly overpressured volume of fluids has a very low connectivity, it cannot exert this pressure in the form of a high flow rate. Therefore, if the permeability is low and ROP high, the formation being drilled at the time the flow is detected is not necessarily the formation from which the flow originates. This was likely the case for the gains observed in wells F04-03, GRK-43, K15-11 and LNS-02.

Another important thing to keep in mind, is that stratigraphic boundaries separate rock of significantly different environments or lithology, while in reality, lithological changes can range from abrupt to gradual vertical and/or lateral transitions. Boundaries separating lithostratigraphic units are sharp and their definition can be arbitrarily chosen. By placing such boundaries in gradually changing lithologies, a bias is imposed. In subsurface work the boundary is usually defined at the highest occurrence of a particular rock type. Suppose formation cuttings were circulated up and determined to be composed of 40% dolomite and 60% anhydrite, then the member would have a name typically containing the word anhydrite. A good example would be the ZEZ1W. Dolomite stringers occur frequently within this unit, which renders its distinction from the ZEZ1C and Z1 Fringe Carbonate Member (ZEZ1F) difficult (**Adrichem-Boogaert & Burgers, 1983**). It is likely that wells K17-02 and TUM-01 experienced a kick that originated from such dolomite stringers in the ZEZ1W. Similarly, the Z3 Anhydrite–Carbonate Member (ZEZ3B) is proposed for those cases where anhydrite intercalations in carbonate and carbonate intercalations in anhydrite render the distinction between the ZEZ3A and ZEZ3C difficult. This suggests that some gains that are classified as having originated from the ZEZ3A might actually be related to carbonates within that member. For example, borehole URE-202 experienced a kick when the bit was still 5 m above the ZEZ3C. However, high GR readings indicate the section did not contain pure anhydrite and could have contained some dolomite.

Correctly classifying intervals is further complicated when few logs are run in a section. Determining the stratigraphy of a section could be based on only cuttings, GR and ROP. When an anhydrite section with massive, low-clay-content dolomite intercalations is drilled, the dolomite's GR and ROP response might not differ much from that of anhydrite. Cuttings are sampled at discrete intervals and as a result the thin layers of dolomite might be overlooked. In addition, if drilling parameters are not carefully checked, a sample may have been taken at the wrong time and therefore wrong depth. Cavings from higher up in the open-hole section could come up as well. In both cases cuttings are correlated with the wrong depth.

It is possible that overpressured zones were drilled without being noticed. If overpressures were encountered and the mud weight had to be increased significantly in order to be able to drill ahead then underlying high-pressure streaks might be drilled without problems. If drilling parameters remained stable it is likely such overpressured zones were overlooked. This might have been the case in well F07-02. Based on the above discussion it can be argued that the amount of kicks originating from carbonate lithologies—and the ZEZ3C in particular—might be higher.

4.2 Seismic Expressions

4.2.1 Visibility of Stringers

Borehole data was correlated with seismic in order to characterise the seismic expressions of forty flowing and nine non-flowing Z3 stringers. Stringers are not resolved on seismic if they are *(i)* too steeply dipping or *(ii)* too thin. In addition, *(iii)* it could be acquisition and processing related. These three parameters will be further explained below on the basis of examples from this study. After that follow two examples of more complex cases, in which the lack of reflectivity is probably a combination of more than one factors.

(i) Four wells penetrated a Z3 stringer with a local dip of more than 45°. It could be determined that the two flowing stringers and the one non-flowing stringer encountered by wells E18-02, GRK-43 and GGT-103 respectively are not resolved on seismic because they are too steeply dipping. On the other hand, the steeply dipping flowing Z3 stringer penetrated by well G18-01 was visible on seismic. This illustrates that the quality of seismic controls the maximum steepness of a stringer's enveloping surface that will be resolved on seismic. Based on these four cases, the minimum dip angle above which a stringer may not be visible on seismic is considered to be 45°. *(ii)* Well F16-A-06-S1 most likely encountered a stringer that is too thin to produce a seismic reflection, based on an increasing GR and decrease in ROP in a 13-m interval. *(iii)* On seismic it seems K07-07 drilled in the vicinity of a salt diapir. The salt appears to have flowed upward into the salt diapir, leaving a pile of stringers—a *stringer graveyard*—with limited halite between individual fragments. If these stringers are in too close proximity to each other, in combination with poor illumination or migration algorithm limitations, these stringers might not be resolved on seismic.

The stringer penetrated by well MKZ-06 is not visible on seismic. The well kicked upon entering the stringer and subsequently had to be abandoned. As a result, the thickness of the stringer could not be determined. However, seismic reveals a shallow-dipping stringer in close proximity of the well path, and uncertainty in well deviation may have affected positioning. This suggests parameter *(ii)* does not apply here, and rather acquisition and processing parameters control the visibility of the stringer in this case.

Well K09AB-B03 encountered several stringers. However, these stringers were only imaged on some of the seismic datasets (see **Appendix C** for comparison of two different seismic datasets, in which one set the stringers are visible and the other set they are not). The seismic dataset in which the Z3 stringers are visible show that the stringers are not steeply dipping. It is therefore likely that the stringers are either too thin *(ii)* or have a too low IA contrast *(iii)* with the surrounding rock to be resolved on one of the datasets.

The discussion of the above examples illustrates that the three parameters dip *(i)*, thickness *(ii)* and AI contrast *(iii)* determine the visibility of a stringer. Seismic quality controls the lower limits of these parameters. In addition, the quality of seismic data is an important factor in the feasibility of predicting overpressures in Z3 stringers based on seismic expressions, as will be discussed in the next section. The discussion above further shows the importance of adequately assessing uncertainty in deviation data. 31 out of 36 (86%) investigated flowing stringers were visible compared to 7 out of 9 (78%) non-flowing stringers. Visibility is therefore a poor indicator for the probability of encountering flowing stringers.

In section **4.1** it became clear that gas generation and disequilibrium compaction through effective isolation of fractured Z3 stringers are the two overpressure mechanisms applicable to the Zechstein. Now that the visibility of stringers is established in this section, three seismic expressions will be presented in the following section which seem to correlate with a higher chance of encountering an overpressured zone. The seismic expressions that are associated with a higher probability of overpressured Z3 stringers include *(1)* low continuity, *(2)* near-edge penetration and *(3)* fold hinges.

4.2.2 Seismic Expressions Correlated with Overpressures

Stringers with *(1)* a low continuity have a higher chance of being completely isolated by impermeable salt, in which case only normal stresses of equal magnitude are applied to the stringers. Low-continuity stringers also have a relatively large surface-area-to-volume ratio and thus have a higher chance of *(2)* being penetrated near their edge. Edges of a stringer represent areas of brittle deformation. Fracture frequency is likely to be higher in these areas, which means there is a higher chance that newly created fractures as a result of brittle failure, connect with the initial fracture network of the carbonate portion of the Z3 stringers and form a permeable zone. It is therefore expected that low-continuity stringers and stringers drilled near their edges have a high probability of exhibiting enhanced permeability and thus the ability to flow. However, this does not exclude non-isolated stringers from flowing.

The vast majority of low-continuity stringers flowed, as did stringers penetrated within 300 m of their edge (**Table 1**). Obviously, the chance of drilling within 300 m of the edge of a low-continuity stringer is higher compared with high-continuity stringers. Despite the clear overlap of these criteria, the two should be regarded as complementary; a high-continuity stringer can be penetrated in the vicinity of its edge as well.

The majority of flowing Z3 stringers were penetrated near *(3)* the hinge of a fold. Higher fracture frequencies in areas of maximum curvature indicate that folding controls fracture frequencies (**Peacock & Mann, 2005**). Additional fractures created when a stringer becomes folded can potentially connect with the initial fracture network near the hinges of a fold to form a permeable fracture network. When combined, the three characteristics 'Low Continuity', 'Edge' and 'Fold Hinge' describe the entire population of flowing Z3 stringers which have been incorporated into the GDE database so far. This does not mean that an isolated stringer that meets one or more of the above criteria always flows. Only when permeability is sufficient—as a result of fracturing—will an isolated stringer flow. This is illustrated by the statistics of the non-flowing stringers, which show that half of them meet 1 out of 3 criteria mentioned above (**Table 1**). On the other hand, it is possible for non-isolated stringers that meet one or more of the above criteria to flow as well, as is illustrated by wells KOL-02, VRS-401 and URE-202 (**Appendix C**).

4.2.3 Other Seismic Expressions Possibly Related to Overpressures

The section below deals with seismic expressions that could possibly be related to higher fracture frequencies and possibly display evidence of overpressures. No statistical analysis was carried out on these seismic features, which deserve further attention in subsequent studies. The wells and seismic features mentioned in the section below can be consulted in **Appendix C**.

Thickened Anhydrite Zones as a Result of Gravity Flows

Van Gent et al. (2010) mention the thickness of Z3 stringers is generally between 30 and 50 m throughout the Southern Permian Basin. This thickness is in accordance with this study (**Appendix B**), which shows a mean Z3 stringer thickness of 54 m (measured along depth, meaning the true vertical depth is less). It is striking that thickened zones are mainly related to thicker anhydrite portions. These thickened anhydrite zones only occur in synclinal structures, where they may form pop-up structures. In this study, such thickened anhydrite zones and pop-up structures were observed on seismic in or near wells BDM-05, H16-01, G18-01, M03-01 and N05-01.

Van Gent et al. (2010) proposed that thickened zones are the product of syn-sedimentary processes. Their preferred scenario involves the formation of depressions after ZEZ4R deposition, in which the creation of an open fracture system in the Z3 allowed brines to circulate into the ZEZ2H. This led to the formation of an extensive network of dissolution channels and collapse of overlying Z3. Sections of the Z3 stringers on the edges of these collapse zones ruptured and slid down the slope—a process known as sediment gravity flow—forming thickened zones.

The model outlined above assumes high relief is present during deposition of the ZE evaporites, in accordance with the classic deep-basin shallow-water model of **Hsü et al. (1973)**. As mentioned in section **1.2.3**, **Van den Belt et al. (2007)** argued that this is an unviable concept and proposed a more elegant evaporite basin model, where isostatic compensation allows the sedimentation of thick evaporite sequences in initially shallow-waters. The shallow-basin shallow-water model of **Van den Belt et al. (2007)** does not involve high relief and therefore, the syn-sedimentary process forming thickened zones as proposed by **Van Gent et al. (2010)** is deemed infeasible.

Sediment gravity flows were observed on seismic near wells G18-01 and GSV-01, whereas boreholes L08-H-02-S1, M03-01 and N05-01-S2 actually penetrated such flows. In all three cases of gravity flow penetrations, (brecciated) claystone cuttings and K–Mg rich salts where observed at the base of what appeared to be a movement zone. In this study it is proposed that thickened zones are simply a result of layer-parallel shortening during halokinesis. As Z3 stringers become folded , the dense, now dipping Z3 stringer will slide down underlying K-Mg salts of the ZEZ2H. These weak and almost fluid-like K–Mg salts form a detachment zone, while clays of the ZEZ3G are smeared along the sliding zone. With sufficient displacement, the brittle anhydrite will tend to break and form pop-up structures to accommodate for the horizontal shortening. The above model explains why thickened anhydrite zones and pop-ups are only observed in synclinal structures.

Erratic Base Loop

The base of sediment gravity flows can be either continuous or discontinuous. Seismic data around boreholes H16-01, N05-01-S1 and N05-01-S3 show a detachment zone that forms a continuous (blue) base loop. In these cases, penetrating such structures did not result in a kick. Borehole N05-01-S2 on the contrary, drilled a discontinuous base loop, after which it gained formation fluids.

The (blue) base loops of the Z3 stringers drilled in wells COV-08-S1, ENA-02, K05-F-02-S1, K17-02 and VRS-401, although not related to sediment gravity flows, display an erratic pattern. Upon penetration, these wells kicked. Erratic base loops of Z3 stringers could indicate that the carbonate portion of the Z3 stringer is fractured, resulting in a higher permeability.

It is important to note that the wells that drilled a continuous base encountered either a thin layer (<5 m) of carbonate or no ZEZ3C at all, whereas most of the wells that penetrated a discontinuous base loop encountered more than 10 m of carbonates. This suggests the thickness of the ZEZ3C determines the width of the displacement zone, and therefore the fracture distribution. Perhaps the more brittle carbonate will not 'slide' as readily as the anhydrite and will tend to fracture instead. It has to be emphasized that further research is required to confirm these correlations.

Faults and Fractures

As described in the previous sections, it is assumed that fault zones represent areas of higher fracture frequencies. It is evident from seismic data that the locations of formation fluid gains in wells COV-08-S1, COV-29, F10-02, K10-17, AME-205, GGT-103, GRK-43, GRO-01, GSV-01, LNS-02, MKZ-06, URE-202 and VRS-401 coincide closely with interpretable fault planes, and thus increased fracture densities. As expected, all wells mentioned above kicked upon drilling near these faulted areas.

Fluid Migration Paths

Fluid migration paths are expressed as thin vertical seismic noise trails. **Ligtenberg (2007)** shows evidence of fluid migration paths that originate from Z3 stringers and all end at the Base Cretaceous Unconformity. In several situations the fluid migration paths occur at fault intersections that are associated with a dominant fault system in the deeper subsurface. It is proposed that these structures are associated with the Late Kimmerian extensional tectonic event. It is further suggested that Z3 stringers with associated fluid migration paths may be (partly) depressurized.

In this study, fluid migration paths may be present near wells F07-02, GGT-103, GRK-43, K11-FA-103 K15-FG-104 and VRS-401. It seems the Z3 stringer encountered by well VRS-401 is leaking fluid upwards along faults that intersect the stringer. This could explain why only soft overpressures (1.45 s.g.) were observed.

4.2.4 Probability Prediction of Overpressures Based on Seismic Expression

In order to assess the risk associated with drilling through stringers, it is important to get an overview of the probability of experiencing a kick when penetrating a Z3 stringer. This means the amount of Z3 stringer penetrations and kicks associated with these stringers must be determined.

Internal databases of both EBN and TNO indicate that a total of 6489 boreholes have been drilled in the Netherlands, as per December 2018. Stratigraphy is defined in 6011 boreholes, of which 2559 drilled through the ZE. Of these ZE penetrations, 2031 were drilled deep enough to encounter the Z3 stringer, if present. The amount of conclusive boreholes was established by determining the number of boreholes that encountered the *Z2 (Stassfurt) Formation*. A total of 1321 boreholes penetrated a Z3 stringer, of which 40 flowed. This suggests only 3% of the tapped Z3 stringer population was overpressured. However, drilling events have been identified and incorporated into the GDE database for only 960 boreholes, as per January

2019. The selection of wells that were analysed is not based on a thorough screening of all 2559 wells that drilled through the ZE. Only 173 wells that are incorporated into the GDE database penetrated a Z3 stringer. Assuming this group of wells is representative for the total population of Z3 stringer penetrations, then 23% of Z3 stringer penetrations resulted in a kick. However, a large number of wells were analysed for events based on expert knowledge, and as such this percentage is an overestimation.

In addition, the total population of Z3 stringer hits is based on the amount of wells that penetrated the corresponding stratigraphies according to NLOG. It is expected that as stratigraphy is updated, the amount of Z3 stringer penetrations will increase. For example, wells E10-03-S2, F10-03, K05-F-02-S1, K09AB-B-03, K09AB-B-03-S1, K10-17, K12-15 and K12-15-S1 encountered a stringer even though the 'officially' defined stratigraphy according to NLOG at this depth is 'Zechstein Group', or, in the case of wells K07-07, K07-07-S2 and K11-FA-103, 'UNKNOWN'. This suggests the population of Z3 stringer penetrations should be bigger, which results in a lower percentage of Z3 stringer kicks.

The 3% of stringer kicks is regarded as a low estimate of all events that occurred during drilling of the Z3 stringers in the Netherlands. This number is expected to go up as more wells that penetrated Z3 stringers are analysed. In fact, **Appendix A** shows a list of potential wells that are not yet incorporated into the GDE database and likely experienced ZE kicks, based on data from NLOG and **Zijp et al., 2018**. However, it may be entirely possible that the actual percentage of stringer kicks is even lower than 3%.

The probability of encountering a kick while drilling through different Z3 stringer configurations is illustrated in **Fig. 4.3**. These configurations and probabilities are based on the seismic expressions related to a kick, as encountered by the wells investigated in this study. As this research deals with existing wells that penetrated the Z3 stringer, $P_{hit} = 100\%$ and therefore, only P_{kick} must be considered. The green, orange and red colour coding, as indicated in the bottom right corner of the figure, represent the probability of encountering hard overpressures (>1.6 s.g., **Loucks et al., 1973**) of 0.1%, 1% and 10% respectively. These kick probabilities are rough estimates based on the assumption that the 3% of Z3 stringer kicks described above is representative for the entire population. Below follows a description of the different configurations.

a) Well H16-01 penetrated a Z3 stringer with a gentle synclinal shape. The thickened anhydrite portion of 180 m formed a pop-up structure, while the 3-m-thick ZEZ3C formed a continuous base. No kick took place while drilling this Z3 stringer configuration, and therefore, the probability of taking a kick in said configuration is assumed to be low. ***b***) Well URE-202 drilled a faulted Z3 stringer that is connected to the overburden. The faulting points towards a higher fracture density. Indeed, the well kicked while drilling halfway through the ZEZ3A. However, only soft overpressures (1.25 s.g.) were observed, which is probably because the stringer is connected to the overburden. In addition, anhydrite is thought to exhibit lower permeabilities, which is translated into lower pore pressures according to Skempton's *B* coefficient. The chance of encountering hard overpressures in Z3 stringers connected to the overburden is considered to be small. ***c***) Well COV-29 tapped a small-sized (~0.15 km^2) Z3 stringer. Seismic data reveals fault planes near the Z3 stringer, which likely contributed to further breaking up the intra salt beds into smaller chunks and to increased fracturing within the stringer. As a result, very hard overpressures (2.32 s.g.) where observed while drilling into this Z3 stringer. Thus, the likelihood of encountering hard overpressures within small-sized Z3 stringers is expected to be high. ***d***) Well K17-02 drilled a Z3 stringer that forms an open anticlinal structure.

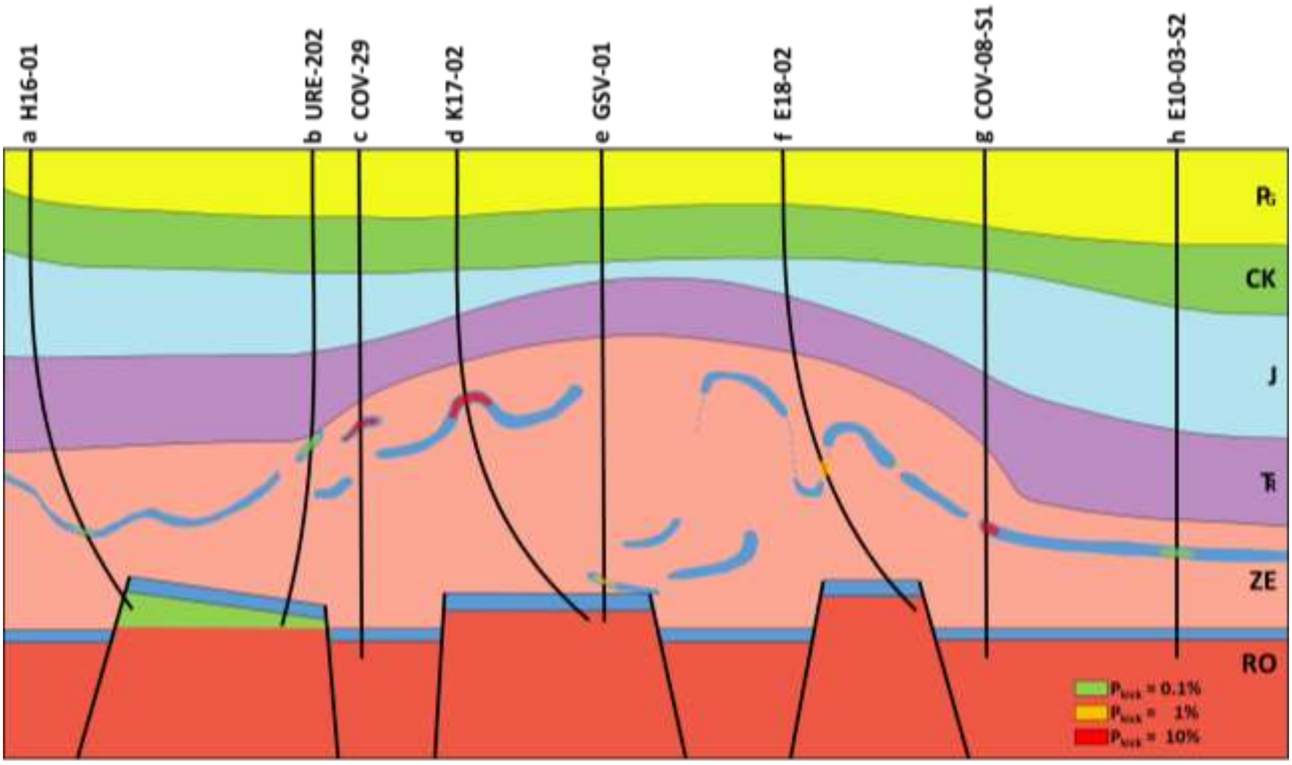

Fig. 4.3 Schematic illustration of Z3 stringer penetrations in different configurations. The colour codes in the bottom right corner represent the likelihood of encountering hard overpressures (>1.8 s.g.) while drilling the different stringer configurations. In this figure it is assumed $P_{hit} = 100\%$ and therefore, only P_{kick} must be considered. Wells represent examples of drilled stringer configurations as encountered in this study. ***a***) Well H16-01 drilled a gentle synclinal structure with a thickened ZEZ3A forming a pop-up structure. The thin ZEZ3C formed a continuous base. ***b***) Well URE-202 drilled a Z3 stringer that is connected to the overburden. ***c***) Well COV-29 drilled a small-sized stringer. ***d***) Well K17-02 drilled an open anticlinal structure. The thick ZEZ3C forms a discontinuous base. ***e***) Well GSV-01 drilled Z3 stringer that is connected to the underburden. ***f***) Well E18-02 drilled a well that is too steeply dipping to be resolved on seismic. ***g***) Well COV-08-S1 drilled the edge of a Z3 stringer. ***h***) Well E10-03-S2 drilled the centre of a continuous, relatively undeformed Z3 stringer.

Higher fracture densities are expected near hinge zones. The erratic (blue) base loop of the stringer further suggests the 66 m thick ZEZ3C is fractured. As expected, hard overpressures (1.9 s.g.) were observed as the well kicked. The probability of experiencing a kick in the Z3 stringer configuration described above is deemed to be high. ***e***) Well GSV-01 drilled a faulted Z3 stringer that is connected to the underburden. As a result, no kick was taken while drilling this Z3 stringer. Although there is a small chance of encountering hard overpressures in Z3 stringers connected to the underburden, it is not recommended to aim for Z3 stringers that appear to be in connection with the underburden based on seismic. From the seismic data in this study it appeared that boreholes AME-203, F10-03, GSV-01, K08-FA-307, L06-07, L08-H-02 and L08-H-02-S1 drilled Z3 stringers overlain by halite and in connection with the underburden. However, well data indicates that wells AME-203, F10-03 and L06-07 found ZEZ2H to be separating Z3 stringers from the underburden. Of these three wells, only F10-03 kicked (with hard overpressures) while drilling through the stringer. Of course, along a different trajectory the stringers may still be connected to the basal ZE. K08-FA-307 had to be abandoned after penetrating the Z3 stringer and is therefore inconclusive to whether the stringer is connected to the underburden or not. From well data it then follows that only boreholes GSV-01, L08-H-02 and L08-H-02-S1 drilled a Z3 stringer that is directly connected to the underburden. Out of these three boreholes, one kicked and observed hard overpressures in the Z3 stringer. To conclude, it is urged to be cautious when aiming for Z3 stringers that appear on seismic to be connected to the underburden, as it may still be isolated by a (thin) layer of ZEZ2H. Therefore, the likelihood of encountering hard overpressures in Z3 stringers connected to the deeper subsurface based on seismic data is considered to be medium. ***f***) Well E18-02 drilled a Z3 stringer that is too steeply dipping to produce a seismic reflection. Since the seismic expressions of an invisible stringer cannot be determined, it seems impractical to establish the probability of encountering a kick in such Z3 stringer configurations. However, since the local dip of a stringer is thought to be a proxy for the amount of deformation a Z3 stringer has experienced, the assumption can be made that there is a medium probability of observing hard overpressures in 'invisible' Z3 stringers. ***g***) Well COV-08-S1 drilled the edge of a continuous Z3 stringer. The edges appear to be faulted, which points towards a higher fracture frequency. As a result, hard overpressures (1.86 s.g.) were observed as the well gained formation fluids. A high probability of a kick is expected when drilling near the edge of a stringer. ***h***) Well E10-03-S2 penetrated a continuous (>10 km^2) Z3 stringer that exhibits a low degree of folding. As such, no kick was taken while drilling through this stringer. The chance of observing hard overpressures in said Z3 stringer configuration is regarded as small.

The probabilities of experiencing a kick while drilling the above Z3 stringer configurations can be taken into account when planning future well trajectories. This might help reduce the time and costs related to anomalous pressures and associated well control situations. Note that for some of the Z3 stringer configurations—such as the stringer connected to the overburden—treated above, only a handful of examples were identified in this study. It is therefore recommended to enlarge the group of identified Z3 stringer kicks to make the statistics more robust. In addition, the group of nine non-flowing Z3 stringers that were analysed in this study is considered to be too small to be representative for the entire population of penetrated stringers that did not kick and should thus be enlarged. It should be emphasized that the above conclusions are drawn from the forty flowing and nine none-flowing Z3 stringer penetrations identified and investigated in this study. New correlations may emerge as more cases are researched.

5. Conclusions

1. The Dutch state entity EBN set up a database that records GDE's that took place during drilling activities in the Netherlands. The goal of the database is to reduce NPT and costs related to GDE's. Sixty-two boreholes were newly examined for the GDE database as part of this study. In addition, GDE descriptions of forty-four wells already incorporated into the database were improved. As per January 2019, the database included 960 wells with 1171 GDE's recorded.
2. The GDE database contained a set of sixty-eight fluid formation gains that took place in the Zechstein. These kicks were imported into Petrel software where the well data was visualized on seismic data, with the goal to investigate whether it is possible to predict overpressures in the ZE based on seismic expressions.
3. The majority (59%) of ZE kicks originated from Z3 stringers and another significant (16%) segment of overpressures were observed in the ZEZ2C. In total, the carbonate members of the ZE accounted for 66% of the kicks. Almost half (39%) of the wells experienced a gas kick, of which 77% were related to the ZE carbonate members. Seismic expressions of Z3 stringers that are correlated to a high chance of encountering hard overpressures include *(i)* a small size (<1 km^2), *(ii)* areas of maximum curvature and *(iii)* areas within 300 m of a stringer's edge. A lithostatic gradient of 2.0–2.3 bar/10 m is representative for the Dutch subsurface, based on density data from five wells that were investigated in this study. ZE overpressures show a depth-related trend and most plot near the lithostatic.
4. Overpressures in the ZE are generated through effective sealing of fractured Z3 stringers and kerogen conversion. Skempton's *B* coefficient describes how most of the vertical load of the overburden is carried by the pores of fractured intra-salt beds. Small-sized Z3 stringers, hinge zones, and areas within 300 m of a Z3 stringer's edge represent areas with increased fracture frequency, resulting in hard overpressures.
5. Internal databases of EBN and TNO revealed that the total population of Z3 stringers penetrated in the Netherlands amounts to 1321, which translates to 3% Z3 stringer kicks. However, the group of forty Z3 stringer kicks identified in this study is based on analyses of 960 boreholes that are incorporated into the GDE database, as of January 2019. Of these boreholes, only 173 encountered a Z3 stringer, from which follows that 23% of the Z3 stringer penetrations must have resulted in a kick. Incompleteness and bias in respectively the internal databases and the wells selected to be incorporated into the GDE database are the cause of these divergent outcomes. The actual percentage of Z3 stringer penetrations that resulted in a kick is expected to lie between these two extremes.
6. The probabilities of taking a kick when penetrating the different Z3 stringer configurations presented in this study may be taken into account when planning future wells. Avoiding these areas may help reduce both NPT and costs while drilling and guarantee safety on the rig. It should be emphasized that the inferences in this report are based on cases of Z3 stringer kicks investigated so far. New insights might arise as more Z3 stringer kicks are identified and investigated.

Recommendations

- Expand the GDE database to get a representative dataset that is suitable for statistically sound analysis. As per January 2019, the database included 960 wells with 1171 GDE's recorded. The ultimate goal is to include up to one third of the 6489 wells drilled in the Netherlands. Only wells drilled for E&P purposes and after 1980 should be included. It is recommended to start by analysing wells in the lists in **Appendix A**, as these likely contain more ZE gains and high-severity GDE's. It is expected that more Z3 stringer kicks will be identified. Visualizing these on seismic could further improve the statistics of seismic expressions related to overpressures in Z3 stringers. In addition, it would improve the statistics on the probability of encountering issues when drilling Z3 stringers and better constrain drilling risks.
- The group of non-flowing Z3 stringers should be expanded to represent a significant set of the total population of Z3 stringer penetrations, which amounts to 1321. This allows to test the validity of the proposed predictions of overpressures in Z3 stringers based on seismic expressions.
- Gain a better understanding of salt deformation with the use of high-quality seismic EBN has at its disposal (4Quads and GEMS 3D seismic cubes). The high quality of the seismic allows for further investigation of the thickened anhydrite zones, gravity flows and faults observed within Z3 stringers. In addition, potential leak-paths might be identified. Assess in detail with the aid of these seismic cubes why some Z3 stringers penetrations (G18-01 and N05-01-S2) resulted in a kick and others not (H16-01, M03-01, N04-02, N05-01-S1, N05-01-S3, N07-04, N07-04A and N07-04A-S1).
- Investigate conditions in which the fracture propagation pressure of shales is higher than that of halite, in order to assess the viability of the shale-capped brine chamber concept.
- Well reports could be scanned to check if any repeat formation tests and leak-off tests were performed on the ZE intervals that kicked. The pressures that resulted from these tests could then be compared to the mud weights used to drill these interval. This data can be used to assess whether it is possible to predict the formation strength of Z3 stringers, in order to prevent mud losses. When overweighting drilling mud in order to regain well control after a kick is taken, fractures are induced in a stringer that may connect compartments that were previously isolated. This may create a permeable fracture network throughout the stringer, which leads to more gains and, possibly, the early abandonment of a well.

Acknowledgements

First and foremost, I would like to express my gratitude to John Verbeek (VU) and Guido Hoetz (EBN) for their supervision and for giving me the opportunity to carry out this MSc thesis. I am grateful to Gert Lammers (WellSpec), Pieter Slabbekoorn (EBN) and Guido Hoetz who taught me a lot about drilling processes and incidents related to drilling. Special thanks to Walter Eikelenboom (EBN), Marten ter Borgh (EBN) and Martin Ecclestone (EBN) for helping me with Petrel software. My report benefited considerably from discussions with Martin Ecclestone, Guido Hoetz, Douwe van Leverink (EBN), Kees van Ojik (EBN) and John Verbeek. Marc Hettema's (EBN) invaluable input on geomechanics is greatly appreciated. Financial support was realized by EBN, where the actual research was conducted. EBN is also thanked for providing the data and Schlumberger is thanked for providing Petrel 2016 under academic license. And last but not least, I would like to express my sincere thanks to fellow interns Jessica Klop, Victor Larède, Alex Marks, Patrick Reinhard and Vibhuti Wani for six great months and their help along the way.

References

Van Adrichem-Boogaert, H.A., 1976. Outline of the Rotliegend (Lower Permian) in The Netherlands – In: Falke, H. (ed.): *The continental Permian in Central, West, and South Europe*, 23–37.

Van Adrichem-Boogaert, H.A. & Burgers, W.F.J., 1983. The development of the Zechstein in The Netherlands. Geologie en Mijnbouw, vol. 62, 83–92.

Van Adrichem-Boogaert, H. A. & Kouwe, W. F. P. 1993–1997. Stratigraphic nomenclature of the Netherlands; revision and update by RGD and NOGEPA. TNO-NITG. *Mededelingen Rijks Geologische Dienst*, Haarlem, vol. 50, 1–37.

Baud, A., 2018. Analyses and seismic integration of the Geo-Drilling Events Database: Predicting losses of drilling fluids using a statistical approach. Internship report, EBN and Utrecht University (not published).

Van den Belt, F.J.G. (2007). *Sedimentary cycles in coal and evaporite basins and the reconstruction of Palaeozoic climate*. PhD. Utrecht University.

Brooks, J., Goff, J.C. & Van Hoorn, B., (eds), 1986. *Habitat of Palaeozoic Gas in N.W. Europe*. Geological Society Special Publication, vol. 23, 121–149.

Diegel, F.A., Schuster, D.C., Karlo, J.F., Schoup, R.C., and Tauvers, P.R., 1995. Cenozoic structural evolution and tectonostratigraphic framework of the northern Gulf Coast continental margin. In: Jackson, M.P.A. (ed), *Salt Tectonics: A Global Perspective*, AAPG Memoir 65; 109–151.

Downey, M. W., 1984. Evaluating seals for hydrocarbon accumulations: AAPG Bulletin, vol. 68, 1752–1763.

Fredrich, J. T., Coblentz, D. D. et al., 2003. *Stress perturbations adjacent to salt bodies in the deepwater Gulf of Mexico*: *SPE 84554*. SPE Annual Technical Conference and Exhibition, Denver, CO, Society of Petroleum Engineers.

Gaarenstroom L, Tromp R.A.J., de Jong M.C., Brandenburg A., 1993. Overpressures in the Central North Sea – Implications for trap integrity and drilling safety. In: Parker, J.R. (ed), *Proceedings of the 4th Conference on Petroleum Geology of Northwest Europe*, Geol. Soc., London, 1305–1313.

Geluk, M.C., 1997. Paleogeographic maps of Moscovian and Artinskian; contributions from the Netherlands. In: Dsoleau, S., De Wever, P. (Eds.), *Peri-thetys Stratigraphic Correlations*, vol. 19. Geodiversitas, 229–234.

Geluk, M.C., 2000. Late Permian (Zechstein) carbonate-facies maps, the Netherlands. *Netherlands Journal of Geosciences/Geologie en Mijnbouw 79(1)*, 17–27.

Geluk, M.C., 2005. Stratigraphy and Tectonics of Permo–Triassic Basins in the Netherlands and Surrounding Areas. Utrecht University.

Geluk, M.C., 2007. Permian. In: Wong, T.E., Batjes, D.A.J., De Jager, J. (Eds.), Geology of the Netherlands. *Royal Netherlands Academy of Arts and Sciences*, Amsterdam, 63–84.

Van Gent, H., Urai, J.L., de Keijzer, M., 2011. The internal geometry of salt structures – A first look using 3D seismic data from the Zechstein of the Netherlands. *Journal of Structural Geology,* vol. 33*(3)*, 292–311.

Haimson, B. and Fairhurst, C., 1967. “Initiation and Extension of Hydraulic Fractures in Rocks.” *Society of Petroleum Engineering Journal*, September: 310–318.

Hangx, S., Spiers, C., & Peach, C., 2009. The mechanical behaviour of anhydrite and the effect of CO2 injection. *Energy Procedia*, vol. *1*(1), 3485–3492.

Hantschel, T., & Kauerauf, A. I., 2009. *Fundamentals of basin and petroleum systems modelling*. Springer Science & Business Media.

Hoetz, G., Jaarsma, B., & Kortekaas, M., 2013, September. Drilling hazards inventory: The key to safer-and cheaper-wells. In *SPE Annual Technical Conference and Exhibition*. Society of Petroleum Engineers.

Hoetz, G., 2016. Observations from Systematic Depth Conversion Reviews-Biased Depth Estimates and the Impact on the Drilling Portfolio. In *78th EAGE Conference and Exhibition*, May 2016.

Hsü, K.J., Cita, M.B., & Ryan, W.B.F., 1973. Late Miocene desiccation of the Mediterranean: Nature, vol. 242, 240–244.

Jackson, M. P., & Hudec, M. R., 2017. *Salt tectonics: Principles and practice*. Cambridge University Press.

De Jager, J. 2007. Geological development. In: Wong, T. E., Batjes, D. A. J. & de Jager, J. (eds.), *Geology of the Netherlands*, Royal Netherlands Academy of Arts and Sciences, Amsterdam, 5–26.

Krijgsman, W., Hilgen, F.J., Raffi, I., Sierro, F.J., & Wilson, D.S., 1999. Chronology, causes and progression of the Messinian salinity crisis: Nature, vol. 400, 652–655.

Kuiper, M.E., 2017. Analysis and inventory of Geo-Drilling Events in the Dutch subsurface; a TIBCO Spotfire interface application. Internship report, EBN and Utrecht University (not published).

Kukla, P. A., Reuning, L., Becker, S., Urai, J. L. & Schoenherr, J. 2011. Distribution and mechanisms of overpressure generation and deflation in the late Neoproterozoic to early Cambrian South Oman Salt Basin. *Geofluids*, vol 11*(4)*, 349–361.

Liang, W., Yang, C., Zhao, Y., Dusseault, M.B. & Liu, J., 2007. Experimental investigation of mechanical properties of bedded salt rock, *International Journal of Rock Mechanics and Mining Sciences*, vol. 44, 400–411.

Liang, W. G., Zhao, Y. S., Xu, S. G., & Dusseault, M. B., 2011. Effect of strain rate on the mechanical properties of salt rock. *International Journal of Rock Mechanics and Mining Sciences*, vol. *1*(48), 161–167.

Liu, X., Xiong, J., & Liang, L., 2015. Investigation of pore structure and fractal characteristics of organic-rich Yanchang formation shale in central China by nitrogen adsorption/desorption analysis. *Journal of Natural Gas Science and Engineering*, *22*, 62–72.

Ligtenberg, J.H., 2007. Indications for Pressure Release from Zechstein Rafts during Late Kimmerian – Implications for Reducing Drilling Risks. EAGE 69th Conference & Exhibition – London, UK, 11–14 June 2007.

Loucks, R. G., Dodge, M. M., & Galloway, W. E., 1979.*Sandstone consolidation analysis to delineate areas of high-quality reservoirs suitable for production of geopressured geothermal energy along the Texas Gulf Coast* (No. ORO-5554-1). Texas University, Austin (USA). Bureau of Economic Geology.

Menning, M., 1995. A numerical time scale for the Permian and Triassic periods: an integrated time analysis. In: Scholle, P.A., Peryt T. & Ulmer-Scholle D.S. (eds) *The Permian of northern Pangea*, vol. 1, Springer Verlag (Berlin), 77–97.

NLOG, 2018. Public online database – oil and gas exploration and production in the Netherlands and the Dutch sector of the North Sea continental shelf: http://www.nlog.nl.

Norman, S.E., & Chase, C.G., 1986. Uplift of the shores of the western Mediterranean due to Messinian desiccation and flexural isostacy: Nature, vol. 322, 450–451.

Peacock, D.C.P. & Mann, A. 2005. Evaluation of the controls on fracturing in reservoir rocks. *Journal of Petroleum Geology*, vol. 28, 385–396.

Schoenherr, Johannes & Urai, Janos & Kukla, Peter & Littke, Ralf & Schléder, Zsolt & Larroque, Jean-Michel & Newall, Mark & Al-Abry, Nadia & A. Al-Siyabi, Hisham & Rawahi, Zuwena, 2007. Limits to the sealing capacity of rock salt: A case study of the Infra-Cambrian Ara Salt from the South Oman Salt Basin. *American Association of Petroleum Geologists bulletin*, vol. 91*(11)*, 1541–1557.

Skempton, A. W., 1954. The pore-pressure coefficients A and B. *Geotechnique*, vol. *4*(4), 143–147.

Slabbekoorn, P., 2018. Draft figures for Focus 2018. Unpublished.

Sone, H., 2012. Mechanical Properties of Shale Gas Reservoir Rocks and its Relation to the in-situ Stress Variation Observed in Shale Gas Reservoirs. Stanford University.

Stan-Kłeczek, I., 2016. The study of the elastic properties of carbonate rocks on a base of laboratory and field measurement. *Acta Montanistica Slovaca*, vol. *21*(1), 76–83.

Strozyk, F., Van Gent, J.L., Urai, J.L. & Kukla, P.A., 2012. 3D seismic study of complex intra-salt deformation: An example from the Upper Permian Zechstein 3 stringer, western Dutch offshore. In Alsop, G.I., Archer, S.G., Hartley, A.J., Grant, N.T. & Hodgkinson, R. (eds), *Salt Tectonics, Sediments and Prospectivity*. Geological Society, London, Special Publications, vol. 363, 489–501.

Taylor, J.C.M., 1998. Upper Permian, Zechstein, in Glennie, K.W. (ed), *Petroleum Geology of the North Sea; Basic Concepts and Recent Advances*, Oxford, Blackwell, 174–210.

Tingay, M.R.P., Morley, C.K., Laird, A., Limpornpipat, O., Krisadasima, K., Pabchanda, S. & Macintyr, H.R., 2013. Evidence for overpressure generation by kerogen-to-gas maturation in the northern Malay Basin. *American Association of Petroleum Geologists bulletin*, vol. 97*(4)*, 639–672.

Warren, J. K., 2016. *Evaporites: A Geological Compendium*. Springer.

Watts, A.B., 2001. Isostasy and Flexure of the Lithosphere: Cambridge, Cambridge University Press, p. 458.

Van Wees, J.D., Stephenson, R.A., Ziegler, P.A., et al., 2000. On the origin of the Southern Permian Basin, Central Europe: Marine and Petroleum Geology, vol. 17, 43–59.

Wennberg, O.P., Casini, G., Jonoud, S. & Peacock, D., 2016. The characteristics of open fractures in carbonate reservoirs and their impact on fluid flow: A discussion. *Petroleum Geoscience*, vol. 22, 91–104.

Zhang, J., Standifird, W.B., Lenamond, C., 2008. Casing ultradeep, ultralong salt sections in deep water: a case study for failure diagnosis and risk mitigation in record-depth well. In *SPE annual technical conference and exhibition*, 21–24 September, Denver, CO, USA.

Zhang J., Wieseneck J., 2011. Challenges and surprises of abnormal pore pressure in shale gas formations. In *SPE annual technical conference and exhibition*, 30 October–2 November, Denver, CO, USA.

Zhang, J., & Yin, S. X., 2017. Fracture gradient prediction: an overview and an improved method. *Petroleum Science*, vol. *14*(4), 720–730.

Zhang, Y. & Zhang, J.J., 2017. Lithology-dependent minimum horizontal stress and in-situ stress estimate. *Tectonophysics*, vol. 703–704, 1–8.

Ziegler, P.A., 1990. Geological Atlas of Western and Central Europe. Shell Internationale Petroleum Maatschappij, Den Haag, p. 239.

Zimmerman, R.W., 1991. Introduction to Poroelasticity Theory. In *Compressibility of Sandstones*. Developments in Petroleum Science, vol. 29, 66–77.

Zijp, M.H.A.A., Huijgen, M.A., Wilpshaar, M., Bouroullec, R. & ter Heege, J.H., 2018. Stringers in Salt as a Drilling Risk. TNO report carried out at the request of State Supervisory of Mines (SodM).

Zoback, M., 2007. Reservoir Geomechanics. Stanford University.

Appendix A

List of wells analysed for the GDE database for the first time:

E18-02	L08-11	L09-01
L07-H-03	L08-12	L09-02
L07-H-03-S1	L08-14	L09-03
L07-N-01	L08-14-S1	L09-04
L07-N-01-S1	L08-15	L09-04-S1
L07-N-02	L08-16	L09-05
L08-01	L08-16-S1	L09-05-S1
L08-01-S1	L08-G-03	L09-06
L08-02	L08-G-03-S1	L09-06-S1
L08-03	L08-G-03-S2	L09-07
L08-04	L08-H-02	L09-07-S1
L08-05	L08-H-02-S1	L09-08
L08-05-S1	L08-P-01	LNS-02
L08-G-01	L08-P-01-S1	K08-FA-307
L08-06	L08-P-02	KOL-02
L08-06-S1	L08-P-03	TVN-01
L08-07	L08-P-03-S1	URE-202
L08-07-S1	L08-P-05	VRS-401
L08-09	L08-P-05-S1	
L08-H-01	L08-P4-01	
L08-10	L08-P4-01-S1	
L08-10-S1	L08-P4-01-S2	

List of wells already in the GDE database on which adjustments were made:

BUMA-01

COV-08-S1

COV-58

E10-03-S2

F04-03

F07-02

F10-02

F10-03

F16-A-06-S1

GRK-43

GRO-01-S1

GSV-01

K02-A-01

K05-F-02-S1

K07-07

K07-07-S2

K07-08

K07-13

K08-FA-308

K08-FA-308-S1

K08-FA-308-S2

K09AB-B-03

K09AB-B-03-S1

K09AB-B-03-S2

K09AB-B-03-S3

K09AB-B-03-S4

K09AB-B-03-S5

K09AB-B-03-S6

K09AB-B-03-S7

K10-17

K12-15

K12-15-S1

K12-15-S2

K15-11

K15-FG-104

K15-FG-104-S1

K17-02

L04-PN-04

L04-PN-04-S1

L06-07

LNS-02

M03-01

MKZ-06

TVN-01

List of wells that likely encountered Zechstein kicks and are recommended to be analysed first (based on NLOG pressure map page and TNO's 'Stringer in Salt' Report):

B17-04	K11-03	J06-A-05
E09-01	K11-04	L04-06
E13-01	K11-10	L13-FH-101
K05-ENC-02	K12-C5-S1	L16-12
K08-02	K14-05	WIT-03
K10-01	K15-13-S1	

List of 10% slowest wells drilled during the period 2007–2017 that are not incorporated into the GDE database yet, which likely experienced high-severity events:

F17-08-S1	K02-A-04-S3	K12-C-05-S1
F17-10	K05-11-S1	L10-36-S2
G14-B-03-S1	K05-CU-02	L15-A-107-S1
G14-B-04	K12-18	ZND-11-S2
G14-B-04-S1	K12-18-S2	
G16-A-03	K12-19-S1	

Appendix B

Time–Depth Relation Per Well (Offshore)		
Wells	**Depth-to-Time Conversion Based On**	**Remarks**
D15-04	TWT Surfaces by TNO	
E10-03-S2	TWT Surfaces by TNO	
E17-02	Check-shots	
E18-02	TWT Surfaces by TNO	
F04-03	TWT Surfaces by TNO	
F04-03	TWT Surfaces by TNO	
F07-02	Check-shots Calibrated with Sonic	
F10-02	Check-shots	Close to a salt dome giving T–D relation a higher uncertainty
F10-03	Check-shots	
F10-03	Check-shots	
F16-A-06-S1	TWT Surfaces by TNO	
G18-01	TWT Surfaces by TNO	
K05-F-02-S1	TWT Surfaces by TNO	ZE well top too deep
K07-07	TWT Surfaces by TNO	No deviation data for the 2831–3096 m interval
K07-07-S2	TWT Surfaces by TNO	
K07-08	Check-shots Calibrated with Sonic	
K07-08	Check-shots Calibrated with Sonic	
K07-13	TWT Surfaces by TNO	ZE and RO well tops too shallow
K08-FA-307	Manually Picked Horizons	
K08-FA-308	Manually Picked Horizons	
K08-FA-308-S1	Manually Picked Horizons	
K08-FA-308-S2	Manually Picked Horizons	
K09AB-B-03	Manually Picked Horizons	
K09AB-B-03-S1	Manually Picked Horizons	
K10-17	TWT Surfaces by TNO	Well drilled close to fault with large offsets, therefore T–D relation uncertain
K11-FA-103	TWT Surfaces by TNO	RO well top possibly too shallow, ZE well top not availably
K12-15	TWT Surfaces by TNO	
K12-15-S1	TWT Surfaces by TNO	
K15-11	TWT Surfaces by TNO	
K15-FG-104	Manually Picked Horizons	ZE well top too deep and RO not available
K15-FG-104-S1	Manually Picked Horizons	ZE well top too deep and RO not available
K17-02	TWT Surfaces by TNO	
K17-02	TWT Surfaces by TNO	
L04-PN-04	TWT Surfaces by TNO	
L04-PN-04-S1	TWT Surfaces by TNO	
L04-PN-04-S1	TWT Surfaces by TNO	
L06-07	TWT Surfaces by TNO	ZE and RO well tops too shallow
L08-H-02	TWT Surfaces by TNO	ZE well top not available, RO too deep
L08-H-02-S1	TWT Surfaces by TNO	ZE well top not available, RO too deep
M03-01	TWT Surfaces by TNO	
N05-01-S2	Inapliccable	Seismic in depth domain

Time–Depth Relation Per Well (Onshore)

Wells	Depth-to-Time Conversion Based On	Remarks
AME-203	TWT Surfaces by TNO	
AME-205	Inapliccable	Seismic in depth domain
BDM-05	TWT Surfaces by TNO	ZE and RO well tops too shallow
BUMA-01	TWT Surfaces by TNO	
COV-08-S1	TWT Surfaces by TNO	
COV-29	TWT Surfaces by TNO	
COV-48-S2	TWT Surfaces by TNO	
COV-58	TWT Surfaces by TNO	
ENA-02	TWT Surfaces by TNO	
GGT-103	Manually Picked Horizons	Well drilled close to faults with large offsets, therefore T–D relation uncertain
GRK-43	TWT Surfaces by TNO	RO well top is too deep
GRO-01	Inapliccable	Seismic in depth domain
GSV-01	TWT Surfaces by TNO	
GTV-01-S1	TWT Surfaces by TNO	
KOL-02	TWT Surfaces by TNO	
LNS-02	TWT Surfaces by TNO	
LNS-02	TWT Surfaces by TNO	
LWZ-03-S1	Manually Picked Horizons	
MKZ-06	TWT Surfaces by TNO	
OPK-01	TWT Surfaces by TNO	
STK-01-S3	TWT Surfaces by TNO	
TUM-01	Manually Picked Horizons	
TVN-01	Manually Picked Horizons	
URE-202	TWT Surfaces by TNO	
VRS-401	TWT Surfaces by TNO	
WYK-06	TWT Surfaces by TNO	
ZWD-02-S1	TWT Surfaces by TNO	

Legend (Kicks)

Column	Field Name	Description
1	Well Name	Well Name as per NLOG
2	Severity	Impact of gain classified as Low - Medium - High as per Appendix
3	Stratigraphy (NLOG)	Stratigraphy as per NLOG
4	GDE Depth (TVD)	GDE Z coordinate (TVDSS or TVDNAP, calculated from MD depth, Kelly Bushing Height and deviation table NLOG)
5	GDE Depth (MD)	Depth (MD with respect to Kelly Bushing) of top interval gain
6	T–D Relation	Classified as Poor -Fair - Good when wells are visualised in the time domain, inapplicable looking at seismic in depth domain
7	Stratigraphy (Interpreted)	Stratigraphy deduced from well logs, seismic and reports
8	Stringer Thickness (MD)	Thickness of Z3 stringer in m as measured along hole
9	ZEZ3A Thickness (MD)	Thickness of Z3 Main Anhydrite Member in m as measured along hole
10	ZEZ3C Thickness (MD)	Thickness of Z3 Carbonate Member in m as measured along hole
11	ZEZ3B Thickness (MD)	Thickness of Z3 Anhydrite/Carbonate Member in m as measured along hole
12	ZEZ3G Thickness (MD)	Thickness of Z3 Grey Salt Clay Member in m as measured along hole
13	ZEZ2T Thickness	Thickness of Z2 Roof Anhydrite Member in m as measured along hole
14	Top ZEZ3A (MD)	Depth in mMD at which top Z3 Anhydrite Member was encountered
15	Top ZEZ3C (MD)	Depth in mMD at which top Z3 Carbonate Member was encountered
16	Top ZEZ3B (MD)	Depth in mMD at which top Z3 Anhydrite/Carbonate Member was encountered
17	Top ZEZ3G (MD)	Depth in mMD at which top Z3 Grey Salt Clay Member was encountered
18	Top ZEZ2T (MD)	Depth in mMD at which top Z2 Roof Anhydrite Member was encountered
19	Top ZE–Stringer Distance (MD)	Distance in mMD between top ZE and Z3 string as measured along hole as per NLOG
20	Top ZE–Gain Distance (MD)	Distance in mMD between top ZE and depth of gain as measured along hole
21	Top ZE–Gain Distance (TVD)	Distance in TVD between top Zechstein and depth of gain
22	Top ZE (MD)	Depth in mMD at which top Zechstein was encountered
23	Top ZE (TVD)	Depth in TVDss at which top Zechstein was encountered
24	Top RO (MD)	Depth in mMD at which top Upper Rotliegendes was encountered
25	Top RO (TVD)	Depth in TVDss at which top Upper Rotliegendes was encountered
27	Fluid Type	Fluid type as described in well reports and classified as Brine - Gas - H2S - Undefined
28	Volume	Minimum volume (in m3) of gain as recorded in well reports
29	Concentration	Highest gas reading as recorded (in ppm) in well reports
30	Kill Mud Gradient	Equivalent mud weight (in s.g.) of gain or mud weight (in s.g.) used to kill well as recorded in well reports
31	Pore Fluid Pressure	Maximum pore fluid pressure in bar as measured in the borehole
31	Cube	Name of 3D Seismic Cubes or 2D lines used as per Studio Petrel MasterNetherlands(_Onshore)
32	Data Quality	Quality of seismic data classified as Poor - Fair - Good
33	Stringer Gain?	Classified as 'Yes' in case gain originated from the Z3 Stringer, cell left blank otherwise
34	Visibility	Visibility of Stringer classified as Low - Medium - High
35	Continuity	Continuity of Stringer classified as Low - Medium - High as per Appendix
36	Area	Estimated surface area of stringer in m^2
37	Distance to Edge	Distance to edge of stringer at well location classified as Centre - Near Edge - Edge as per Appendix
38	Dip	Dip angle of stringer classified as Horizontal - Near Horizontal - Dipping - Steep as per Appendix
39	Hinge/Limb	Geometry of stringer at well location classified as Anticline - Limb - Syncline as per Appendix
40	Curvature	Curvature of stringer classified as either None - Concave - Convex
41	Relative Depth	Value in the range of 0–1 which represents the depth (TVDss) at which the gain occurred relative to top and base ZE
42	Relative Depth	Relative depth at which gain occurred within the ZE subdivided in Top ZE - Mid ZE - Base ZE as per Appendix
43	Doubling/Tripling	States if 1 or more stringer intervals was encountered in a borehole
44	Stringer Thickness (ms)	Thickness of stringer (perpendicular to dip) on seismic measured in ms (TWT)
45	Top ZE	Flat - Folded (crest, through, flank) - Faulted
46	Base ZE	Flat - Faulted (down-thrown, pop-up)
47	Z3 Aligned With	States if Z3 stringer geometry follows top or base ZE, or neither, classified as Top ZE - Base ZE - No
48	Comments	Any additional comments regarding gain
49	Domain	Indicates whether seismic on screenshots is in either 'Time' or 'Depth' domain
50	Relative Acoustic Impedance	Gains for which relative acoustic impedance sections are available are denoted with an 'X'

Appendix (Kicks)

Classification	Description
Low Severity	Able to control influx whilst drilling ahead. Increased mud weight to overbalance formation pressure.
Medium Severity	Well control situation requiring well to be circulated to heavier fluid in controlled manner (over the choke). High pressures requiring a contingency liner to be set to allow drilling ahead.
High Severity	Influx exceeding kick tolerance. Gain–Loss situation. Well control situation resulting in >5 days regaining well control. Kick resulting in prematurely setting casing.
Low Continuity	< 1 km^2
Medium Continuity	1–10 km^2
High Continuity	> 10 km^2
Centre	> 1 km from edge
Near Edge	300–1000 m from edge
Edge	Within 300 m of edge
Horizontal	Dipping angle of stringer in the range of 0–5°
Near Horizontal	Dipping angle of stringer in the range of 5–20°
Dipping	Dipping angle of stringer in the range of 20–45°
Steep	Dipping angle of stringer in the range of 45–90°
Anticline	Within 300 m of crest
Limb	When more than 300 m away from apex
Syncline	Within 300 m of trough
Top ZE	Depth of Stringer relative to Top and Base ZE with values in column 41 in the range of 0–0.35
Mid ZE	Depth of Stringer relative to Top and Base ZE with values in column 41 in the range of 0.35–0.65
Base ZE	Depth of Stringer relative to Top and Base ZE with values in column 41 in the range of 0.65–1

Legend (Lithostatic Gradient)

Classification	Description
	Extrapolated values.
	North Sea (assumed 10 °C seawater with 35‰ salinity and density of 1027 kg/m^3) estimated depths using public bathymetry maps.
	Density used from WRV-01 well. (G18-01, H16-01, K06-D-01, K15/03 and WRV-01 all encountered similar members at similar depths above the MMU (Rupel Formation), which means their densities are considered as similar for this purpose)! The Upper North Sea sediments have not been compacted and uplifted like the underlying sediments.
	Density data from H16-01 used to fill in the 'gaps of G18-01 (wells G18-01 and H16-01 are in close proximity of each other and encountered the same lithologies).
	Gap in density log inferred from composite log (showing halite = 2.1).
	Density data from K06-D-01 used to fill in the 'gaps' of K15-03. They encountered similar Upper North Sea Supergroup sediments.

Appendix C

Page number list of screenshots per well as included in PowerPoint file (named Appendix C):

Flowing Offshore Wells

Well	Page
D15-04	2
E10-03-S2	8
E17-02	12
E18-02	19
F04-03	26
F07-02	35
F10-02	40
F10-03	46
F16-A-06-S1	53
G18-01	59
K05-F-02-S1	68
K07-07	72
K07-07-S2	72
K07-08	82
K07-13	92
K08-FA-307	96
K08-FA-308	101
K08-FA-308-S1	101
K08-FA-308-S2	101
K09AB-B-03	110
K09AB-B-03-S1	110
K10-17	114
K11-FA-103	118
K12-15	123
K12-15-S1	123
K15-11	128
K15-FG-104	133
K15-FG-104-S1	133
K17-02	138
L04-PN-04	142
L04-PN-04-S1	142
L06-07	155
L08-H-02	159
L08-H-02-S1	159
M03-01	165
N05-01-S2	170

Flowing Onshore Wells

Well	Page
AME-203	179
AME-205	185
BDM-05	191
BUMA-01	197
COV-08-S1	204
COV-29	208
COV-48-S2	214
COV-58	223
ENA-02	229
GGT-103	233
GRK-43	237
GRO-01	243
GSV-01	248
GTV-01-S1	253
KOL-02	258
LNS-02	264
LWZ-03-S1	268
MKZ-06	272
OPK-01	279
STK-01-S3	284
TUM-01	288
TVN-01	294
URE-202	300
VRS-401	305
WYK-06	310
ZWD-02-S1	313

Non-Flowing Z3 Stringers

Well	Page
AME-203	318
BDM-05	324
H16-01	331
E10-03-S2	339
F07-02	345
GGT-103	351
K15-11	356
LWZ-03-S1	364
TUM-01	368